

Journal of Science and Technology in The Tropics

Volume 11 Number 2 Dec 2015

CONTENTS

Signal Hearability For Location Determination Techniques (LDT) Using GSM And UMTS Network <i>Norsuzila Y, Mohd Shahir M. Rosli, Akmarulnizam Z, Azita L. Yusof, Darmawaty M. Ali and Azlina I</i>	45
Major Geomagnetic Storms and Relation with Plasma Parameters, Interplanetary Magnetic Field Parameters, and Geomagnetic Index during Solar Cycle <i>Norsuzila Yaa'cob, Nur Syaahidah.M, Akmarulnizam Z and Azita Laily Y</i>	55
Performance Evaluation of Interference Alignment (IA) Scheme in Mobile Wimax Application Using Equalization Algorithm <i>Nor Azlizan Hussien, Azlina Idris and Azita Laily</i>	65
Livestock Information System using Android based Architecture <i>M.H. Ariff, I. Ismarani and N. Shamsuddin</i>	73
Differentiating Ischemic Stroke Severity Using Artificial Neural Network <i>Omar WRW, Mohamad Z, Taib MN and Jailani R</i>	84
Humanoid Robot Navigation in Human Environment <i>Zulkifli Mohamed and Genci Capi</i>	94

Signal Hearability For Location Determination Techniques (LDT) Using GSM And UMTS Network

Norsuzila Y¹, Mohd Shahir M. Rosli², Akmarulnizam Z³, Azita L. Yusof⁴,
Darmawaty M. Ali⁵, Azlina I⁶

¹ Wireless Communication Technology Group (WiCoT), Faculty of Electrical Engineering, Universiti Teknologi MARA, 40450 Shah Alam, Selangor, Malaysia

²Faculty of Electrical Engineering, Universiti Teknologi MARA (UiTM), Shah Alam, Selangor, Malaysia

(*corresponding Author: norsuzilayaacob@yahoo.com)

Received: 30.05.15; accepted: 05.07.15

Abstract Localization or famously known as Location Determination Technique (LDT) is an information service, which is accessible with mobile devices through the mobile network and which uses information on the geographical position of the mobile device. In order to ensure the LDT works accordingly at any locations, parameter so called hearability is a very important parameter to be considered. Therefore this paper presented the analysis of signal hearability along the main road inside University Technology of MARA (UiTM), Shah Alam. Based on data recorded by NEMO Outdoor during measurement campaign, the result shows that no low hearability signal detected in General System for Mobile communications (GSM) network and several locations found with low hearability in Universal Mobile Telecommunication System (UMTS) network. In addition, the Global Positioning System (GPS) signals are available along the main road.

Keywords Location Determination Technique- GSM- UMTS- GPS- Hearability

INTRODUCTION

Location based service (LBS) started in United States of America (USA) where US (United States) Federal Communication Commission (FCC) requires that the precise location of all enhanced 911 (E911) callers be automatically determined since most of the callers are coming from mobile phones [1]. The requirement from FCC was to determine the location of MS within accuracy of 100m [2]. According to this needs, LBS system has been developed in parallel with the advancement of cellular system, as this technology will be beneficial to many different public and enterprise. Location of Mobile Station (MS) can be determined by implementing LDT with the availability of cellular network [3]. However, there were lots of techniques can be use to determine the MS position. Generally these techniques are divided into two categories such network based and terminal based. For network based approaches the network will do the measurement by collecting few parameters and use them to calculate and estimate the position of MS. Thus no changes at MS are required. Meanwhile for terminal based approaches MS will do the calculation and not depending on the network [4].

In addition, GPS and Assisted Global Positioning System (A-GPS) can be used to determine the location of MS as well. The position of MS cannot be located unless the MS able to detect signals from at least 3 Base Station (BS) and it also known as signal

hearability. In cellular telecommunications network, in order to reduce the interferences to other MS which reside in the same cell or adjacent cell the minimum power transmitted will be always used. Therefore the hearability for MS is getting lower when MS residing at the centre or in a large cell. This issue is more critical in UMTS network where UMTS has a tight power control scheme [5, 6]. These research objectives are to collect GSM, UMTS and GPS data and analyse signal hearability. Then propose appropriate localization technique in UiTM especially at low hearability area.

METHODOLOGY

Field measurements started with identified the selected route for drive test in UiTM Shah Alam by referring to Google Maps and UiTM map. For this research, Celcom GSM and UMTS network were selected for data collection. Then, data collection was carried out for three times in the morning, evening and night using NEMO Outdoor. Once data collection completed, all data were analysed and appropriate LDT techniques was proposed at UiTM area according to the hearability condition. The summary of the methodology for this research is illustrated in Fig. 1.

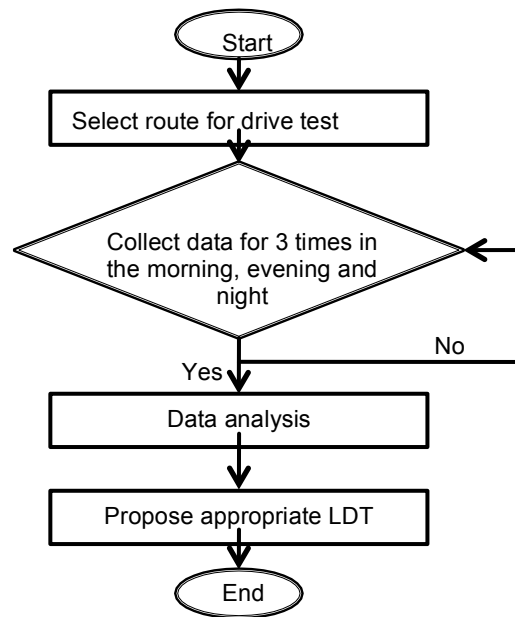


Figure 1. Flow chart of methodology

By referring to Google Maps, the drive test or data collection route has been identified and only main road was covered during the data collection. For data collection, GPS and two Nokia mobile phones were connected to NEMO outdoor which has been installed in laptop. The GPS was placed on vehicle roof while both Nokia phones were placed under the vehicle front screen. Before the measurement campaign started, Nokia phones and GPS was connected to the laptop. Then NEMO Outdoor was initialized and the connection was checked in order to avoid any connection error during the measurement. After successful connection, UiTM map was loaded in NEMO Outdoor, and then one phone was locked in GSM band and the other one locked in UMTS band. Once NEMO outdoor was ready, measurement campaign started and NEMO outdoor is recording all the measurement campaign and saved in the log for further analysis. The distance of measurement campaign

was around 10km and average of vehicle speed is 25 kmh⁻¹. During data collection, GPS monitoring application (GPS Tool Scott Presnell, Tworoads Software, and Version 1.5) has been installed in Blackberry device in order to monitor the GPS signal availability at UiTM main roads. The NEMO Outdoor and Blackberry device were carried out simultaneously during the drive test.

RESULT AND DISCUSSION

GSM drive test

NEMO Outdoor coloured (green, red, and yellow) the route taken in UiTM according to standard GSM signal strength as shown in Fig. 2. The GSM signal strength were in good condition and therefore no low signal strength detected around UiTM main road. The Celcom standard signal strength are Good (≥ -65 dBm), Average (< -85 and ≥ -65), Fair (≥ -95 and ≤ -85) and Poor (< -95).

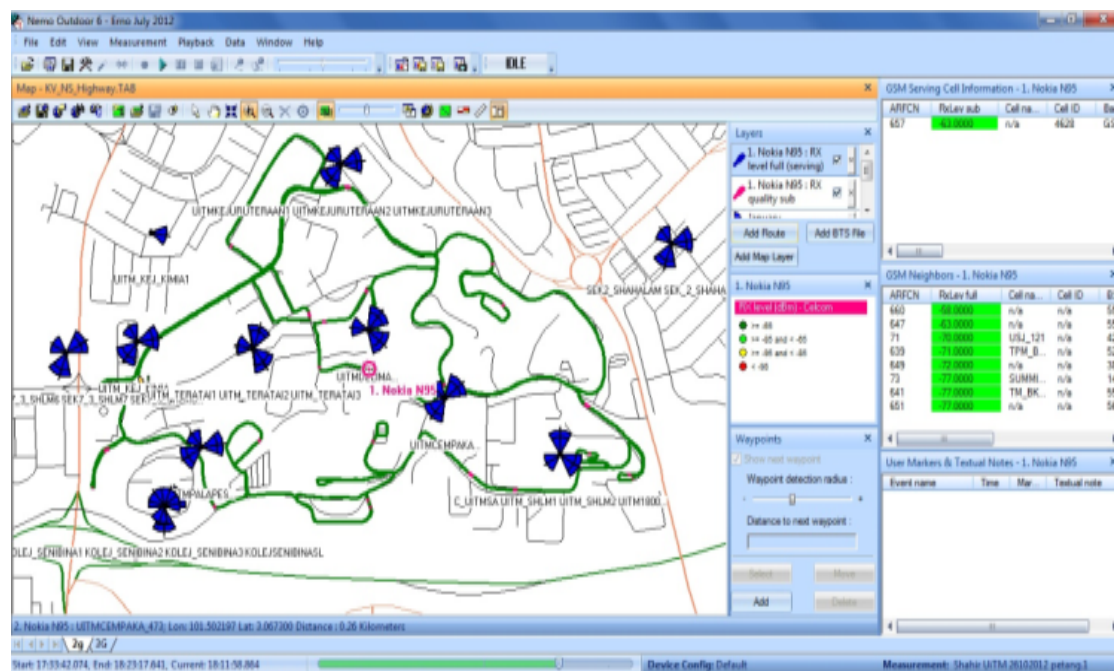
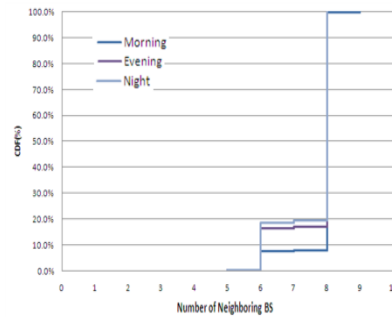


Figure 2. Route for GSM data collection in evening

Next, data from recorded GSM log was analysed using NEMO Analyzer and extracted into Excel sheet as shown in Fig. 3(a). Serving row is referring to the serving BS while Neighbour row is referring to the neighbour BS. Other parameters related to network info captured during measurement campaign can be found in the same table. MS able to get at least six neighbouring BS and the maximum number of neighbouring BS detected was nine neighbouring BS. It shows that signal hearability in UiTM GSM is very good. Same goes to data collection for morning and night, same result was identified. Moreover, average power receives level (Rx Level) for GSM neighbouring BS is -60dBm.

Time	Cell type	Site name	Cell name	Radius (m)	ABSC	BSC	EC	CP	ACC	BAC
S:8:13PM	Serving	UTIM_KEL_KINMAL	UTIM_KEL_KINMAL	52	66	5			100%	1
S:8:13PM	Neighbor	UTIM_TERATAJ	UTIM_TERATAJ	72	870					
S:8:13PM	Neighbor	UTIM_KEL_KINMAL	UTIM_KEL_KINMAL	68	4					
S:8:13PM	Neighbor	UTIM_KEL_KINMAL	UTIM_KEL_KINMAL	61	74					
S:8:13PM	Neighbor	KOLEJ_SEMBINANG	KOLEJ_SEMBINANG	89	73					
S:8:13PM	Neighbor	KOLEJ_SEMBINANG	KOLEJ_SEMBINANG	91	2					
S:8:13PM	Neighbor	SEK_7_SHAHALAMZ	SEK_7_SHAHALAMZ	93	7					
S:8:13PM	Serving	UTIM_KEL_KINMAL	UTIM_KEL_KINMAL	62	66	5			100%	1
S:8:14PM	Neighbor	UTIM_TERATAJ	UTIM_TERATAJ	71	670					
S:8:14PM	Neighbor	UTIM_KEL_KINMAL	UTIM_KEL_KINMAL	68	4					
S:8:14PM	Neighbor	KOLEJ_SEMBINANG	KOLEJ_SEMBINANG	88	2					
S:8:14PM	Neighbor	KOLEJ_SEMBINANG	KOLEJ_SEMBINANG	89	73					
S:8:14PM	Neighbor	SEK_7_SHAHALAMZ	SEK_7_SHAHALAMZ	92	7					
S:8:14PM	Serving	UTIM_KEL_KINMAL	UTIM_KEL_KINMAL	55	66	5			100%	1
S:8:14PM	Neighbor			72	670	11				
S:8:14PM	Neighbor	UTIM_KEL_KINMAL	UTIM_KEL_KINMAL	71	4					
S:8:14PM	Neighbor	C_UTIMSA	UTIM_SHAHAL	78	5					
S:8:14PM	Neighbor	KOLEJ_SEMBINANG	KOLEJ_SEMBINANG	87	2					
S:8:14PM	Neighbor	KOLEJ_SEMBINANG	KOLEJ_SEMBINANG	88	73					
S:8:14PM	Serving	UTIM_KEL_KINMAL	UTIM_KEL_KINMAL	53	66	5			100%	1
S:8:15PM	Neighbor			71	670	11				
S:8:15PM	Neighbor			71	4	58				
S:8:15PM	Neighbor	C_UTIMSA	UTIM_SHAHAL	79	5					
S:8:15PM	Neighbor	KOLEJ_SEMBINANG	KOLEJ_SEMBINANG	87	2					
S:8:15PM	Neighbor	KOLEJ_SEMBINANG	KOLEJ_SEMBINANG	87	71					

(a)



(b)

Figure 3. Extracted GSM by NEMO and CDF of GSM neighbouring set BS

Cumulative Density Function (CDF) was used to identify the percentage of neighbouring BS collected by MS at the respective time. According to morning, evening and night data, 50% of the data shows that MS was able to get eight neighbouring BS as illustrated in Fig. 3b. As for localization technique, two neighbouring cell is sufficient to calculate the MS position. Thus localization in UiTM GSM network is possible. In addition, no low hearability area detected from GSM data.

UMTS drive test

The results for UMTS measurement campaign recorded in NEMO Outdoor are illustrated in Fig. 4. Same goes to GSM, NEMO distinguished the UMTS signal strength (RSCP,dBm) into Very Good (>=-65dBm), Good (<-85dBm and >=-65dBm), Average (<-85dBm and >=-95dBm), Poor (<-95dBm and >=-103dBm) and Very Poor (<-103dBm). Based on conducted drive test the UMTS signal strength in UiTM Shah Alam seems fluctuated between very good (green), good (light green) and average (yellow).

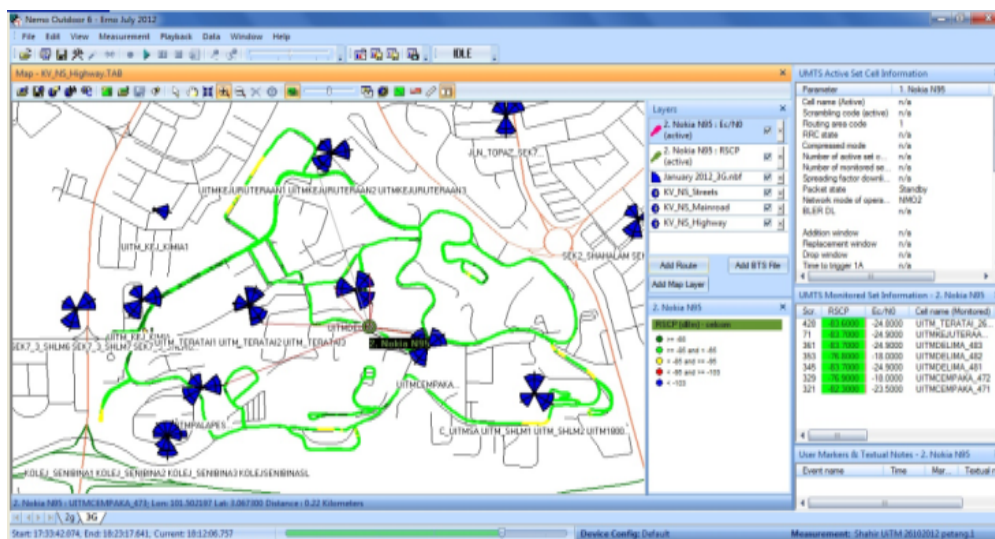


Figure 4. Route for UMTS data collection in evening

Then the data was analysed using NEMO Analyzer and extracted into Excel sheet as shown in Fig. 5a. Same goes to GSM, the active row is referring to the serving BS while monitored row is referring to the neighbour BS. Other parameters related to network info captured during measurement campaign can be found in the same table as well. Based on Fig. 5a, the number of neighbouring cell was not consistent where at some area only one neighbouring cell available and another area might get from two to eight neighbouring cells. Since there were areas detected with one neighbouring cell only, meaning that low hearability area existed in UiTM UMTS network. Besides, average power received (RSCP) for UMTS neighbouring BS is -79 dBm. From CDF data shown in Fig. 5b, 50% shows that MS was able to detect five neighbouring cell during morning, evening and night. For overall, signal hearability in UMTS network still acceptable for localization although there were few area affected with low hearability signal.

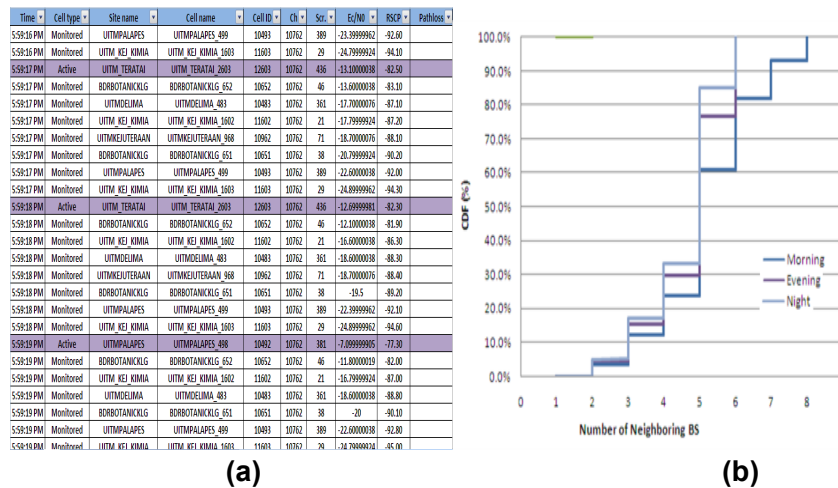


Figure 5. Extracted UMTS data and CDF of UMTS neighboring BS

Low signal hearability has been detected at two locations, which only one neighbouring BS can be heard by MS. Although the signal hearability is low at this area, localization is still possible with the assisted by GPS signal. The affected areas are UiTM swimming pool and from Faculty of Civil Engineering (FKA) to Faculty of Computer and Science (FSKM) as shown in Fig. 6.



Figure 6. UiTM swimming pool and from FKA & FKS

Satellite reception for GSM and UMTS

Since NEMO collected both GSM and UMTS network info at the same time, the same GPS was used to monitor the satellite reception for both GSM and UMTS positioning. By referring to Fig.7, the lowest satellite reception detected by GPS in UiTM during morning data collection is four and the highest is nine. Therefore satellite signal hearability in UiTM Shah Alam is very good and UiTM main road areas are fully covered with satellite signal. As a result, localization using GPS technique should be working at all time.

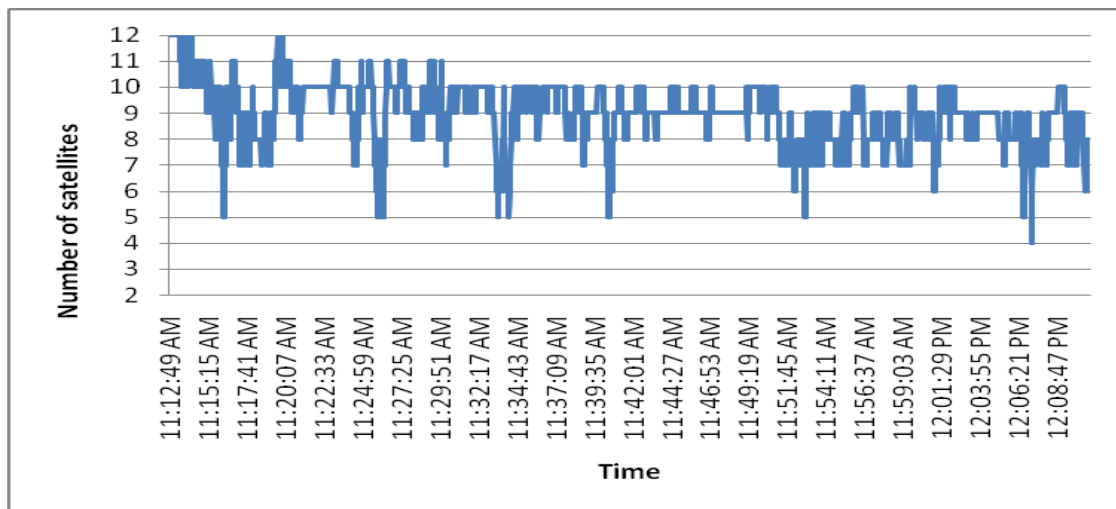


Figure 7. Number of satellite detected

Satellite CDF data illustrated in Fig. 8A. It shows that at 50% nine satellites has been detected throughout the data collection. Furthermore, no low hearability for satellite signals at UiTM main road during morning, evening and night. Plotted coordinates in latitude and longitude for GPS during morning, evening and night are illustrated respectively in Fig.8b.

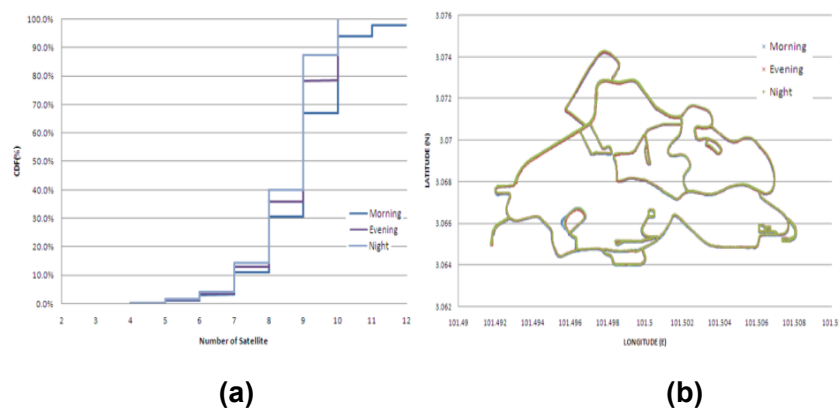


Figure 8. CDF of satellite reception and Plotted coordinates for GPS

Instead of monitored the GPS hearability via NEMO, GPS application was installed in Blackberry device as well and it has been use together during the data collection. As a

results there were no low GPS signal hearability been detected along the main road in UiTM. Therefore this result is tally with the GPS monitored by NEMO. The output of GPS signals monitoring by Blackberry application is illustrated in Fig.9.

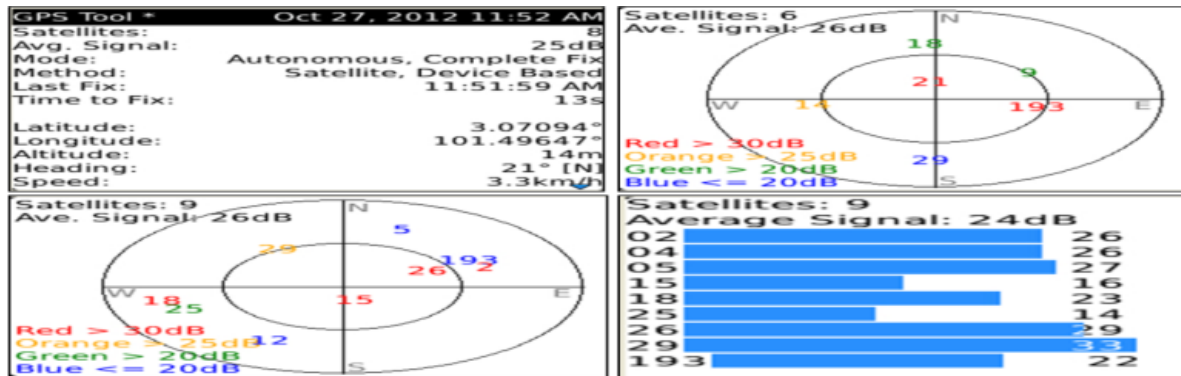


Figure 9. GPS signal monitored by blackberry application

For GSM network in UiTM, there should be no issue to apply the LDT as no hearability issue been detected. Therefore E-OTD method could be applied. In UiTM UMTS network, most of the areas are well covered with sufficient neighbouring BS. Thus network-based localization is possible by using OTDOA method. However there are several locations that unable to hear enough neighbouring BS signal. In consequences, localization using network based is impossible due to low signal hearability. On the other hand, localization can be done by assistance from GPS since GPS signal is available at all main road area. Localization using GPS method can be used in order to resolve the low hearability issue at swimming pool, in front of FSKM and in front of FKA. Summary of the obtained results are summarized in Table 1

Table 1. Summary of signal hearability

Network	GSM	UMTS
Neighbour BS	8	5
Low hearaility	No	Yes
GPS Availability	Yes	Yes
Power received	-60dBm	-79dBm
Proposed LDT	E-OTD&GPS	OTDOA&GPS

Table 2 shows the sample of data collected for UMTS network which contains of time, serving and neighbouring BS, RSCP and path loss value. By referring to path loss value for serving BS, distance between serving BS and MS can be calculated by using Okamura-Hatta path loss model.

Table 2. Data collected for UMTS network

Time	Cell Type	Site Name	RSCP	Pathloss
11:12:52AM	Active	UITM_KEJ_	-61.90	97
11:12:52AM	Monitored	UITM_TERATAI	-72.30	
11:12:52AM	Monitored	UITMDELIMA	-73.10	

Okamura-Hatta path loss model:

(1)

$$L_b = 28.9 + 33.9 \log_{10} f_c + 35.2 \log_{10} d \quad (\text{dB})$$

Where L is the path loss in decibels, f_c is the wavelength and d is the transmitter and receiver distance. As referred to Table 2, path loss (L) is equals to 97dB, therefore d is equals to 0.3km. Then the location of MS can be calculated by using OTDOA formula as per below:

(2)

$$c \times GTD_2 = \sqrt{(x - x_1)^2 + (y - y_1)^2} - \sqrt{(x - x_2)^2 + (y - y_2)^2}$$

$$c \times GTD_3 = \sqrt{(x - x_1)^2 + (y - y_1)^2} - \sqrt{(x - x_3)^2 + (y - y_3)^2}$$

Where;

(3)

$$c \times GTD_2 = d_1 - d_2 = RD_1$$

$$c \times GTD_3 = d_1 - d_3 = RD_2$$

Then MS location can be identified as shown in Fig. 10.

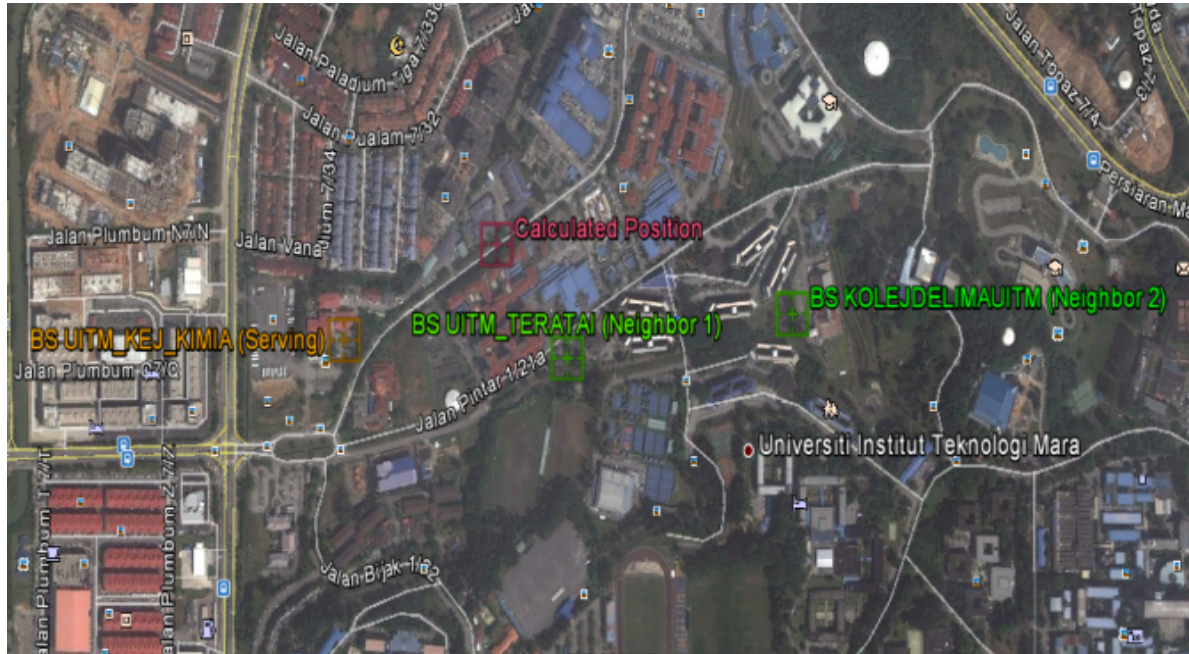


Figure 10. Calculated MS position

CONCLUSION

In this paper signal hearability in UiTM Shah Alam GSM and UMTS network are analysed. No low hearability detected in GSM network but few locations were detected with low hearability. Despite network based positioning can't be used at this area, GPS method is able to overcome the low hearability issue. Moreover GPS signal is available along the main road.

Acknowledgements

The authors would like to thank Faculty of Electrical Engineering, Universiti Teknologi MARA (UiTM) for their valuable support.

REFERENCES

1. Yap. J.H.; Ghaheri-Niri. **S.**; and Tafazolli. R. (2002), Accuracy And Hearability Of Mobile Positioning In GSM And CDMA Networks, 3G Mobile Communication Technologies, 8-10 May 2002. *Conference Publication No. 489 0 IEEE*
2. Alexandra. O.; Tero. H.; and Visa. K. (2015), Cell Hearability Analysis in UTRAN Long Term Evolution Downlink Department of Signal Processing and Acoustics. *SMARAD CoE, Helsinki University of Technology, P.O. Box 3000, FI-02015, TKK, Finland*

3. Sabariah. B.;Mahamod. I.;and Mardina. A. (2010). Simulation model and location accuracy for observed time difference of arrival (OTDOA) positioning in 3G system, *Proceeding of 2010 IEEE Scord 2010, 13th -14th December 2010, Putrajaya Malaysia*
4. Andreas. S.D.(2010). Positioning Technologies and Mechanisms for Mobile Devices, *Seminar Master Module SNET2, TU-Berlin.*
5. Mahamod. I; Ishak.M.; and Mohd. A.M.A. (2011). Availability of GPS and A-GPS signal in UKM Campus for Hearability Check, 2011 IEEE 10th Malaysia International Conference on Communication (MICC) 2nd-5th October 2011, Sutera Harbour Resort, Kota Kinabalu, Sabah, Malaysia
6. Guolin Sun, Jie Chen, Wei Guo and K.J. Ray Liu (2005), Signal Processing Techniques in Network-Aided Positioning. A survey of state-of-the-art positioning designs. *IEEE Signal Processing Magazine July.*

Major Geomagnetic Storms and Relation with Plasma Parameters, Interplanetary Magnetic Field Parameters, and Geomagnetic Index during Solar Cycle

Norsuzila Yaa'cob^{1,2,*}, Nur Syaahidah.M^{1,2}, Akmarulnizam Z^{1,2}, Azita Laily Y^{1,2}

¹Faculty of Electrical Engineering, Universiti Teknologi MARA, 40450 Shah Alam, Selangor DE, Malaysia

²Wireless Communication Technology Group (WiCoT), Faculty of Electrical Engineering, Universiti Teknologi MARA (UiTM), Shah Alam, Selangor, Malaysia

*Corresponding Author: norsuzilayaacob@yahoo.com

Received: 17.06.2015; accepted 30.08.2015

Abstract A geomagnetic storm is a temporary disturbance of the Earth's magnetic field, known as magnetosphere. It usually occurred due to a disturbance in the interplanetary magnetic field (IMF). This paper investigates the relationship that exist among the following IMF parameters: (Bz, By, Bt), and the geomagnetic index (GI): (Kp, Dst, Ap, Ae) along side with the plasma parameters: (T, P, V) during major geomagnetic storms. In this study major geomagnetic storms were indicated by Dst below than -200nT. The data between 1996-1998 and 2004-2006 which are minimum phase of solar cycle 23 while maximum phase is during 2000-2001 were taken from OMNI Web Data Explorer and National Geophysical Data Center. A correlative study between the geomagnetic indices and the peak of various plasma and field parameters during major geomagnetic storms of solar cycle 23 also presented. The result shows that some parameters used have moderate role ($0.3 < r < 0.5$) in Dst morphology and some do not have significant role.

Keywords Geomagnetic storm, geomagnetic index, magnetosphere, interplanetary magnetic field (IMF), plasma

INTRODUCTION

Geomagnetic storm is a temporary disturbance in the Earth's magnetic field caused by coronal mass ejections (CMEs) or solar flare from the Sun. The increase in the solar wind pressure will compress the magnetosphere and the solar wind's magnetic field will interact with the Earth's magnetic field and transfer an increased amount of energy into the magnetosphere [1]. The solar wind carries with it the magnetic field of the Sun and when it enters to the interplanetary medium it is called as interplanetary magnetic field (IMF). The storms generally occurred due to abnormal conditions in the interplanetary magnetic field (IMF) and solar wind plasma emissions caused by various solar phenomenon [2]. The *Bt* value of the IMF indicated the total strength of the IMF. The higher this value, the better it is for enhanced geomagnetic conditions [3]. The IMF is a vector quantity with a three axis

component, two of them (B_x and B_y) are orientated parallel to the ecliptic. The third component, the B_z value is perpendicular to the ecliptic and is created by waves and other disturbances in the solar wind [3]. It is usually assumed that the peak value of the storm, as measured by Dst index, is obtained after the southward component of IMF, B_z has also reached peak value [5].

Geomagnetic index is also related to geomagnetic storms. Geomagnetic index used are K_p index, Dst index, A_e index, and A_p index. The K_p index quantifies disturbances in the horizontal component of Earth's magnetic field. Dst is a measure of the decrease in the horizontal component of the Earth's magnetic field near the magnetic equator due to increases in the magnetospheric ring current. Storms are categorized as major storms if the minimum Dst is below -200nT [2]. A_e index is used to indicate the auroral, or substorm activity. The A_p -index provides a daily average level for geomagnetic activity where days with high levels of geomagnetic activity have a higher daily A_p -value. Solar cycle is that the Sun's hemispheres do not always peak at the same time. The second peak, if it occurs, will likely feature the southern hemisphere playing catch-up, with a surge in activity south of the sun's equator [6]. This paper investigates the relationship that exist among the following IMF parameters and the GI alongside with the plasma parameters during major geomagnetic storms. Then, correlation will be observed between the geomagnetic indices and the peak of various plasma and field parameters during major geomagnetic storms of solar cycle 23.

METHODOLOGY

The data are collected from OMNIWeb. The minima phases taken are during 1996-1999 while maxima phase is from 2000-2002 at solar cycle 23. Figure 1 shows the flowchart of the research methodology.

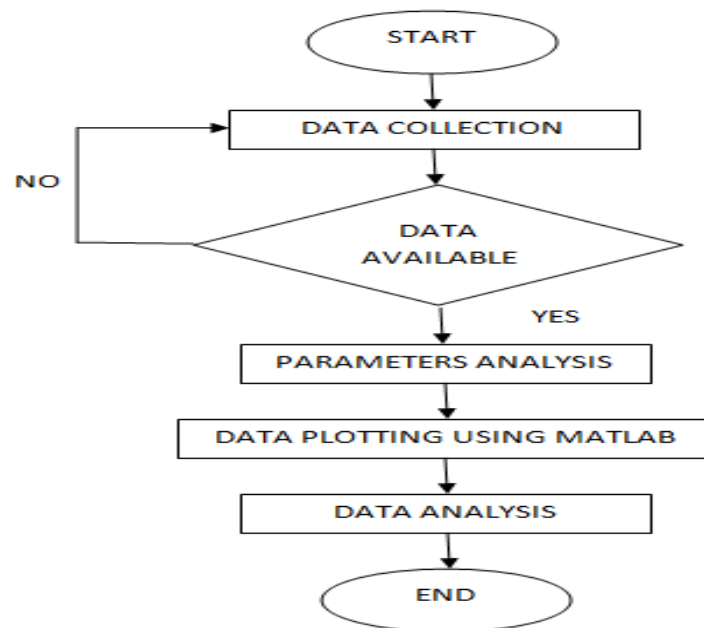


Figure 1. Flowchart of Research

The major storms during maxima and minima are obtained based on the graph with the minimum Dst below -200nT. The parameters are being used to study the major storms: B_t (nT), B_y (nT), B_z (nT). The plasma parameters used are: T (K), D (N/cm³), V (km/s). For geomagnetic index are: K_p , Dst , A_p , and A_e index. Then the parameter were analysed using matlab software. After that analisis the relationship between the storm and IMF, GI, and plasma parameters, the significant major storms during the three periods above are taken by indentifying the exact date of the event. In this study, correlative study has been done to see how strong the relationship between the geomagnetic indices and the peak of various plasma and field parameters during major geomagnetic storms of solar cycle 23. The mathematical formula used for computing r is shown in Eq. 1 where n is the number of pairs of data [7].

Equation 1

$$r = \frac{n \sum xy - (\sum x)(\sum y)}{\sqrt{n(\sum x^2) - (\sum x)^2} \sqrt{n(\sum y^2) - (\sum y)^2}}$$

The strong or weakness the relationship is measured by the value of r . The value of r is such that $-1 \leq r \leq +1$. The + and – signs are used for positive linear correlations and negative

linear correlations, respectively. Positive correlation means if x and y have a strong positive linear correlation, value of r is close to $+1$. Positive values indicate a relationship between x and y such that as values of x increase, values of y also increase. Negative correlation means if x and y have a strong positive linear correlation, value of r is close to -1 . Negative values indicate a relationship between x and y such that as values of x increase, values for y decrease as shown in Figure 2.

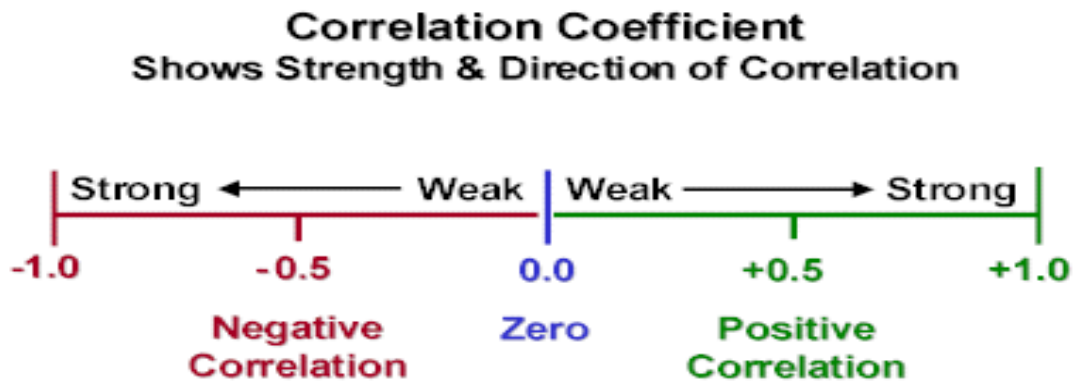


Figure 2. Strength and direction of correlation coefficient

RESULT AND DISCUSSION

Observation period during minima phase 1996-1998

Three major storms occurred from year 1996-1998 based on hourly average. The storms occurred in May 1998 and October 1998 with the largest minimum Dst -205 nT. For minima phase during 1996-1998, the significant event of storm occurred on May 1998, thus the analysis of data is made from 3 May 1998 to 5 May 1998. The data are represented in Figure 3 to 5. During the period of 3 May 1998 to 5 May 1998, major geomagnetic storm occurred on 4 May 1998. Based on Figure 3, there is sudden increment in the readings on 4 May 1998 at 0300 UT for Bt , Bz and By and followed by the Dst index with delay of one hour. The readings for the IMF (Bt , Bz , and By) reached their peak at 0400 UT and Dst reached its peak at 0500 UT. During the main phase of the storm which occurred on 4 May 1998 at 0500 UT with the value of Dst is -205 nT it can be seen that the readings of Bt , Bz , and By started to decrease. The result is obvious; Bz component has growth before the initial phase of geomagnetic storms, which is not during the main phase. This shown time delay between Bz and Dst peak.

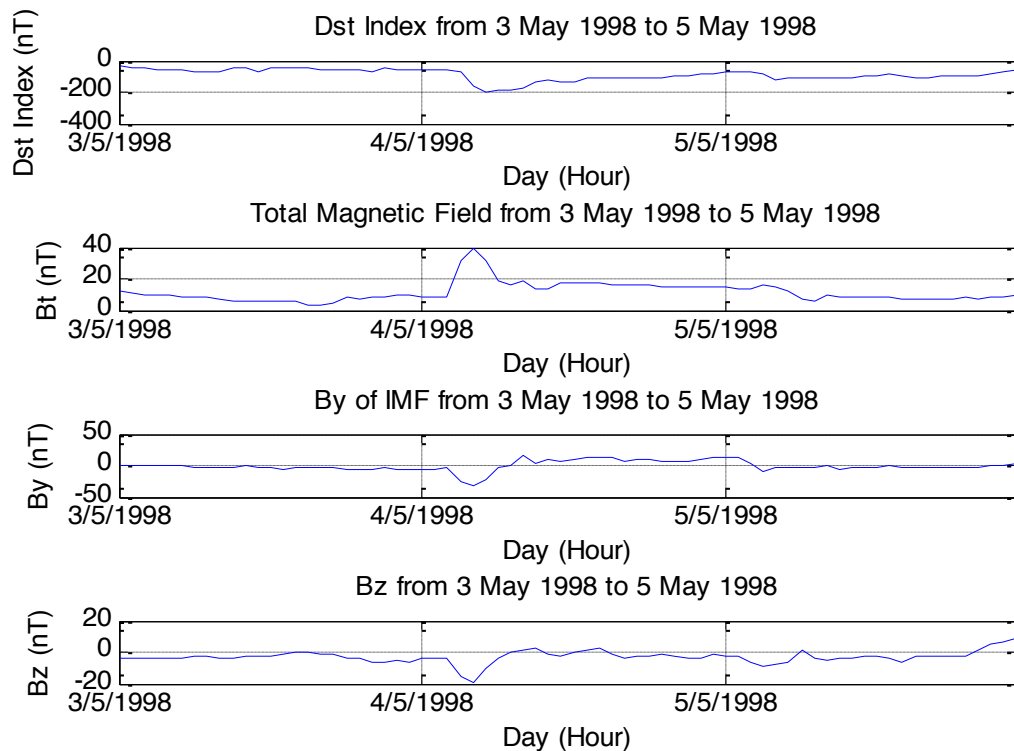


Figure 3. The graph of *Dst* and *Bt*, *By*, and *Bz* from 3 May 1998 to 5 May 1998

From Figure 4, it can be seen that during the main phase of the storm on 4 May 1998, the plasma parameters increase rapidly which signifying the occurrence of the storm. But not all the parameters are at their peak value when *Dst* reached its maximum value at 0500 UT. The plasma speed reached its peak at 0400 UT, the proton temperature reached the maximum value at 0600 UT, while the proton density has fluctuate pattern. Meanwhile, according to Figure 5, during the main phase of storm on 4 May 1998, all the geomagnetic index (*Kp*, *Ap*, *Ae*) increase and considered to show positive peak signifying the storm commencement. Delay of the indices were due to the different latitude location of the index measurements.

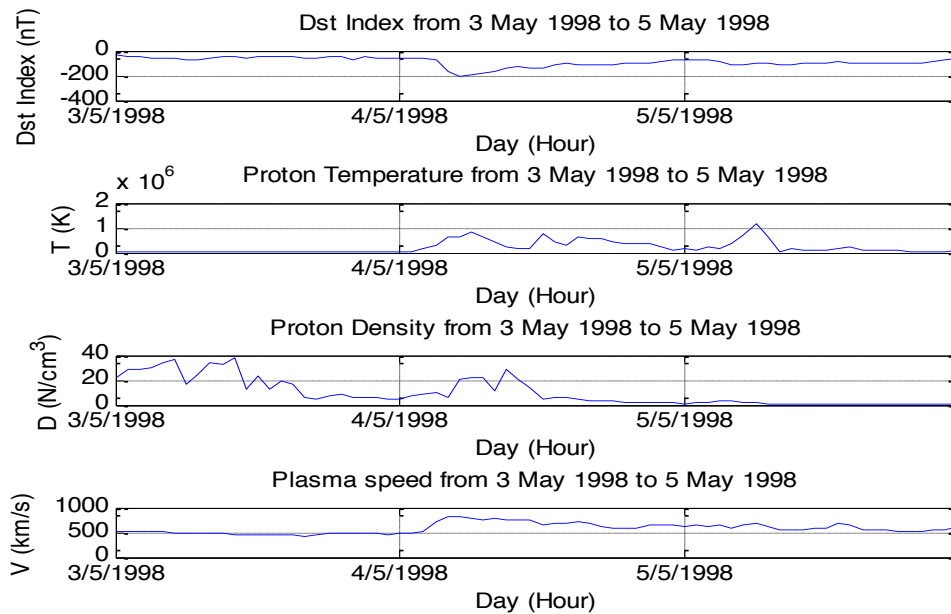


Figure 4. The graph of Dst and T , D , and V from 3 May 1998 to 5 May 1998

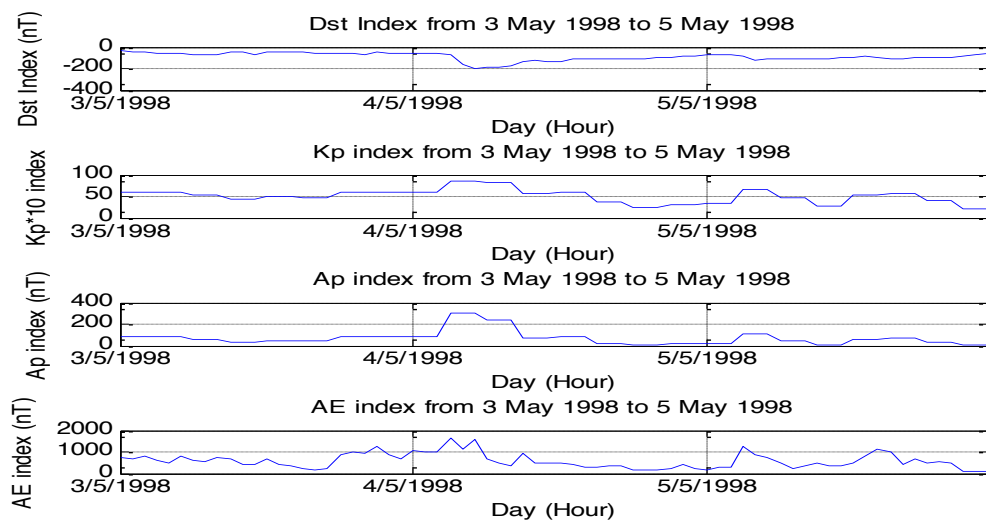


Figure 5. The graph of Dst and Kp , Ap , and Ae from 3 May 1998 to 5 May 1998

Observation period during maxima phase 2000-2002

Fifty six major storms occurred from year 2000-2002 based on hourly average. The major storms actively occurred from 2000-2001 with highest minimum Dst -387 nT. For maxima phase during 2000-2002, the analysis of data is made from 30 March 2001 to 1 April 2001. The data are represented in Figure 6 to 8. From Figure 6, the sudden commencement is seen on 31 March 2001 as this sudden increase in Dst value corresponding increase in Bz was observed. The main phase of the storm is on 31 March 2001 at 0800 UT with the Dst value recorded is -387 nT. The result is obvious Bz component has growth before the initial

phase of geomagnetic storms which is not during the main phase. This shows time delay between B_z and Dst peak.

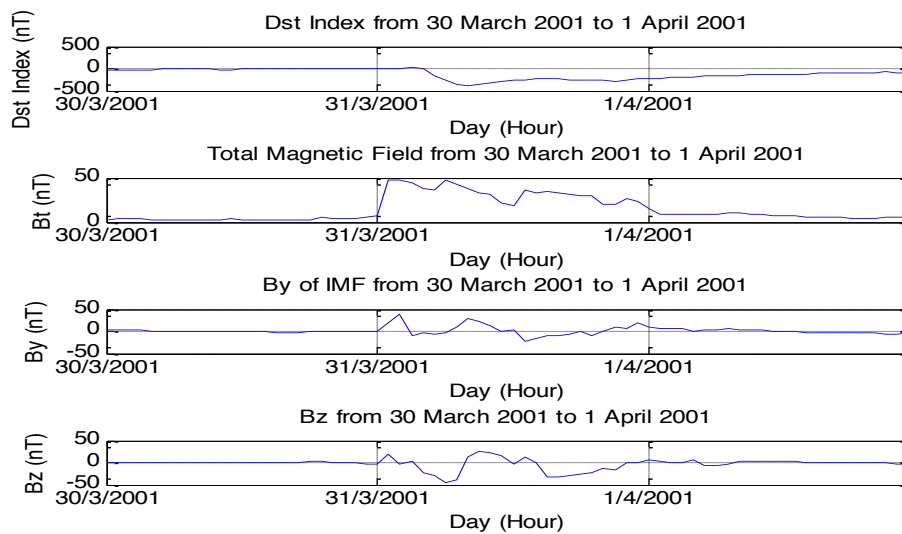


Figure 6. The graph of Dst and B_t , B_y , and B_z from 30 March 2001 to 1 April 2001

Based on Figure 7, it can be seen that during the main phase of the storm on 31 March 2001, only plasma speed can be considered at its peak while the other two parameters show their the minimum values. The behaviour is similar during 2004.

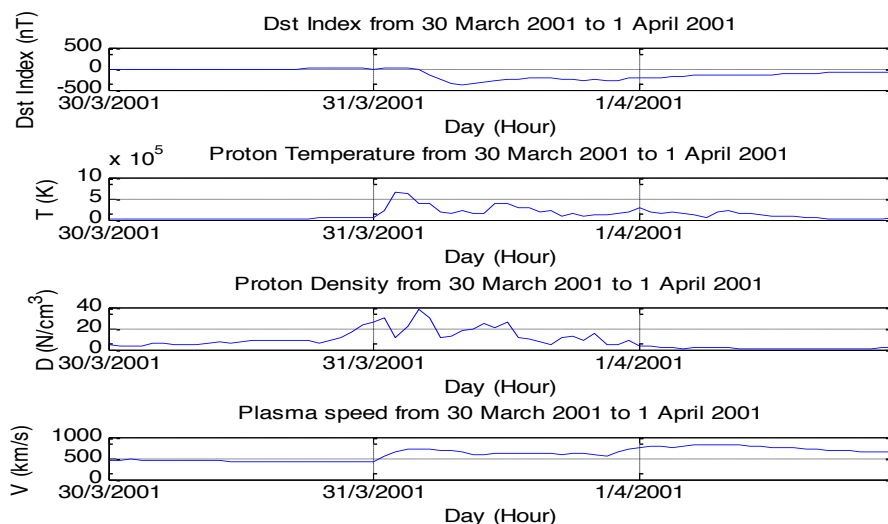


Figure 7. The graph of Dst and T , D , and V from 30 March 2001 to 1 April 2001

According to Figure 8, during the main phase of storm on 31 March 2001, all the geomagnetic index increase and show the positive peak signifying the storm commencement except the A_e index. K_p and A_p index reached the peak at the same time

with *Dst* at 0800 UT while the *Ae* index reached its peak on 31 March 2001 at 1800 UT. Delay of the indices were due to the different latitude location of the index measurements.

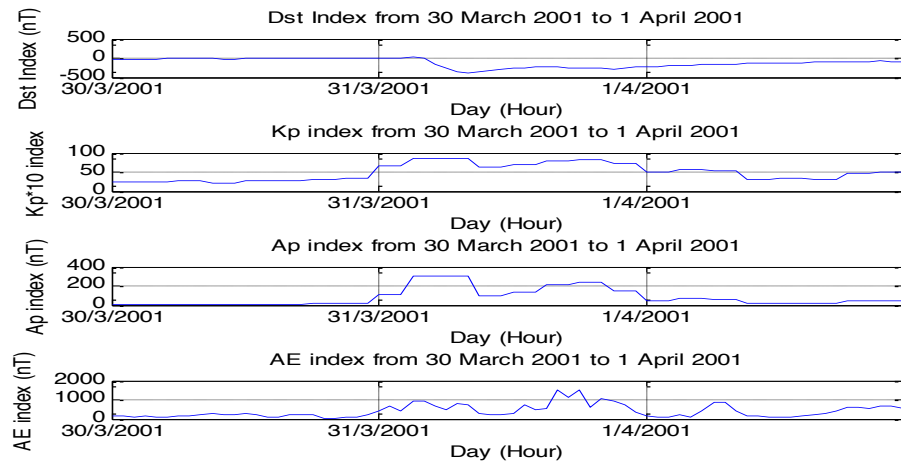


Figure 8. *Dst* and *Kp*, *Ap*, and *Ae* from 30 March 2001 to 1 April 2001

Correlations between Geomagnetic Indices, Field and Plasma Parameters

The correlative coefficient is studied to measure the strength of the relationship between geomagnetic indices, field and plasma parameters. All the data are shown in Table 1, Table 2, and Table 3. From Table 1, it is shown that *Dst* show moderate negative correlation value with *Kp* and *Ap*, and weak negative correlation value with *Ae*. These results represent an anti-phase relationship which means that positive enhancement in geomagnetic index results in increasing negative magnitude of *Dst* that eventually result in major storm. Geomagnetic index are well correlated with each other and it indicates that the three indices can be interchangeably used. This study only interested on the first column of correlation coefficient value which represent the relationship of *Dst* index with geomagnetic index. The other column of it are used as reference.

Table 1. Correlation coefficient between *Dst* and Geomagnetic Index.

	<i>Dst</i>	<i>Kp</i>	<i>Ae</i>	<i>Ap</i>
<i>Dst</i>	1			
<i>Kp</i>	-0.4239043	1		
<i>Ae</i>	-0.1307164	0.58967272	1	
<i>Ap</i>	-0.4543616	0.93950341	0.59970451	1

Table 2 is the result of the correlation between *Dst* index and the field parameters. The *Dst* is not correlated with *By* and weakly negative correlated with *Bt* but moderately correlated with *Bz*. *Bt* also not correlated with *By* and moderately correlated with *Bz*. *Bz* is also not correlated with *By* and moderately correlated with *Bz*. This study only interested on the first column of correlation coefficient value which represent the relationship of *Dst* index with IMF parameters. The other columns of it are used as reference.

Table 2. Correlation coefficient between *Dst* and Field Parameters

	<i>Dst</i>	D	V	K
<i>Dst</i>	1			
D	-0.0331874	1		
V	-0.0488441	0.94315997	1	
K	-0.0515976	0.94460805	0.99905902	1

Based on Table 3, it is seen that *Dst* and all plasma parameters show anti-phase relation with weak negative correlation. But the plasma parameters are well correlated with each other. This study only interested on the first column of correlation coefficient value which represent the relationship of *Dst* index with plasma parameters. The other columns of it are used as reference.

Table 3. Correlation Coefficient between *Dst* and Plasma Parameters

	<i>Dst</i>	<i>Bt</i>	<i>By</i>	<i>Bz</i>
<i>Dst</i>	1			
<i>Bt</i>	-0.1343442	1		
<i>By</i>	0.03815607	0.18017774	1	
<i>Bz</i>	0.30008396	-0.3492673	0.14467784	1

CONCLUSION

It is proven that majority of major storms occurred during maximum phase of solar cycle. Based on the analysis of major geomagnetic storms, it can be seen that there are delays of about 1 to 5 hours between the peak of *Bz* and the peak *Dst* which the peak of the storm's intensity, as measured by the *Dst* index, will occur about 1-5 hours after the driving *Bz* component has reached its peak value. The correlative study done shows that there are no strong correlation between *Dst* index, geomagnetic index, field, and plasma parameters. However, *Kp* index and *Ap* index show moderate negative linear relationship with *Dst* index and could be used to predict geomagnetic storms. The peak of *Dst* is correlated to the maximum negative component of *Bz*. *Bz* component is the strongest connection and better than the solar wind density and solar wind speed [8].

Acknowledgements

The authors would like to thank the Faculty of Electrical Engineering, Universiti Teknologi MARA (UiTM) for their valuable support.

REFERENCES

1. Tripathi, R.; and Mishra, A.P. (2006). Occurrence Of Severe Geomagnetic Storms And Their Association With Solar Interplanetary Features, *ILWS Workshop*,
2. Balveer, S. R.; Subash, C.; Kaushik, K.A.; Firoz, D.C; Gupta, A.K.; Shrivastava, K; Kant, P.; and Ram, M. B.(2011). A Correlative Study of Geomagnetic Storms Associated with Solar Wind and IMF Features During Solar Cycle 23, *International Journal of Applied Physics and Mathematics, vol 1, no 2*.
3. The Interplanetary Magnetic Field-IMF (2014). Retrieved Mei 5, 2014, from <http://www.spaceweatherlive.com/en/help/the-interplanetary-magnetic-field>.
4. Verma, P.L. (2012). Large Geomagnetic Storms And Their Relation With Coronal Mass Ejections And Interplanetary Magnetic Field.
5. Gonzalez, W.D.; and Echer, E. (2005). A Study On The Peak Dst And The Peak Negative Bz Relationship During Intense Geomagnetic Storms. *Geophysical research letters, vol 32*,
6. Tony, P., Solar Cycle Updates – Twin Peaks (2014). Retrieved Mei 16, 2014, from http://science.nasa.gov/science-news/science-at-nasa/2013/01mar_twinp/
7. Pearson Product-Moment Correlation (2014). Retrieved August 16, 2014, from <https://statistics.laerd.com/statistical-guides/pearson-correlation-coefficient-statistical-guide.php>
8. Kaka, O.R.; Bello, O.R.; and Rabi, A.B. (2013). The Variations Of Plasma, Field Parameters And Geomagnetic Index During Geomagnetic Storms Of April 2010. *FUTA Journal of Research in Sciences*
9. Dst Index (2014). Retrieved Mei 16, 2014, from <http://www.aer.com/science-research/space/space-weather/space-weather-index>
10. Le, G.; Russell, C.T.; and Luhmann, J.G. (1997). Polar Magnetic Observations Of The Low Altitude Magnetosphere During The January 1997 Coronal Mass Ejection/Magnetic Cloud Event, *Institute of Geophysics and Planetary Physics, University of California, Los Angeles*

Performance Evaluation of Interference Alignment (IA) Scheme in Mobile Wimax Application Using Equalization Algorithm

Nor Azlizan Hussien, Azlina Idris, Azita Laily

Faculty of Electrical Engineering, Universiti Teknologi Mara, 40450, Shah Alam, Selangor DE, Malaysia.

(*corresponding Author: iazlizan90@gmail.com)

Received: 27.06.2015; accepted: 28.08.2015

Abstract One of the challenges issue in Orthogonal Frequency Division Multiple Access (OFDMA) is the interference of the system, which is the inter-symbol interference (ISI) and inter-carrier interference (ICI) is being considered. So that, in this paper the interference alignment scheme together with the implementation of the Minimum Mean Square Error (MMSE) equalizer is proposed to be adopted in wireless network, OFDMA system. The objective of this study is to evaluate the Pairwise Error Probability (PEP) performance of the presented study and the simulation results show that the PEP performance is improved when implementing the interference alignment, and further improved when implementing the scheme with the MMSE equalizer. The effect of ICI and ISI can be reduced and the maximum diversity of the system is achieved by using the proposed Interference Alignment scheme, and implementation of equalizer.

Keywords Orthogonal Frequency Division Multiple Access, Frequency Division Multiple Access; Interference Alignment;

INTRODUCTION

In future, over a few years later the broadband wireless data services are expected to have apparent growth. OFDM (Orthogonal Frequency Division Multiplexing) provides such high data rate services and considered as a good choice of this matter due to its ability to overcome multipath fading. OFDM is the multiplexing technique that subdivides the available bandwidth into multiple frequency subcarriers. There is a strong interest to extend this OFDM concept to the multiuser communication scenarios, and the best solution of this matter is the Orthogonal Frequency Division Multiple Access (OFDMA).

Currently, the OFDMA has been considered as the multiple access technology by standards for broadband wireless systems, such as 802.16e, 3GPP LTE and 802.20 as the air interface. OFDMA was first introduced for the return channel of cable tv (CTV) networks. Basically, the formation of OFDMA is coming from the combination of OFDM and Frequency Division Multiple Access (FDMA) protocol [1].

This OFDMA transmission technology can be further improved by employing the antenna techniques, called as multiple input multiple output (MIMO). In principle, OFDMA and MIMO can be combined to offer the benefits of simplicity, high performance system [2] and exploitation of the multipath diversity which increases the achievable rate and enhances link reliability [3].

Apart from that, a smart antenna technology known as diversity technique is applied throughout this system. Basically, there are two diversity order system, the Space Time

Block Codes (STBC) and Space Frequency Block Codes (SFBC) while the Space Time Frequency Block Codes (STFBC) is the combination of both technique. The STFBC technique is chosen to be implemented in this study as it gives the advantages of ability to exploit the space, time and frequency domains. This is happen because throughout the coding, the symbols are distributed along the different antennas, time slots and frequency spectrum. OFDMA served many advantages; however there are still disadvantages exists in this system. Since the OFDMA served the available subcarrier for different user, synchronization becomes a difficult task, so the receiver must estimate a number of parameter and hence ISI is induced. Besides, OFDMA is inherit the infirmity of OFDM which is very sensitive to carrier frequency offsets (CFO) and hence induce to the presence of the ICI [4]. These interferences severely degrade the system performance.

Hence, interference alignment (IA) scheme is proposed as a technique to mitigate the ICI, while the implementation of equalizer purposely to reduce the ISI. There were several work done previously, for example in [5], the researcher investigated the Bit Error Rate (BER) for the performance of the system by using the diversity technique of STFBC and implementation of equalizer, but do not employ the interference alignment scheme as the ICI is not being considered in their research.

In [6], the researcher tested the BER performance of the system using STFBC technique with inter-carrier interference self-cancellation scheme (ICI-SC) without the implementation of equalizer as they are aiming to reduce ICI only but not ISI.

Besides, there are a few researchers who have proposed IA together with the implementation of equalizer. For instance, Tresch and Guillaud [7] proposed IA together with a zero-forcing equalizer at the receiver to achieve the sum mutual information, but it is applied in the cellular network. The interference alignment scheme was presented in [8] together with a robust MMSE-based iterative scheme for the wireless network. But there are not considered any diversity technique in their research. The performance evaluation by using pair-wise error probability and linear equalizer for the wireless network has been proposed before. The researcher [9] are considered the diversity technique, but not the IA scheme. So far, there is no literature on performance evaluation of PEP using specific equalization algorithm, IA scheme and diversity order technique (STFBC) in MIMO-OFDMA system, so, this research paper is proposed.

METHODOLOGY

Fig. 1 shows a baseband model of OFDMA system. The block diagram basically comprising of three major parts namely transmitter, channel and receiver. The marked on the block diagram stated the proposed technique approach in this research.

At the transmitter part, the system has parallel transmission paths, each performs serial-to-parallel conversion with the total number of OFDMA subcarrier. After that, the inverse fast Fourier Transform (IFFT) modulates the OFDMA signal before the transmit signals are up-converted to RF signal and being transmitted. Then, the data is delivered to cyclic prefix to mitigate ISI effect if the length of cyclic prefix is $\frac{1}{4}$ of the length of symbol [10].

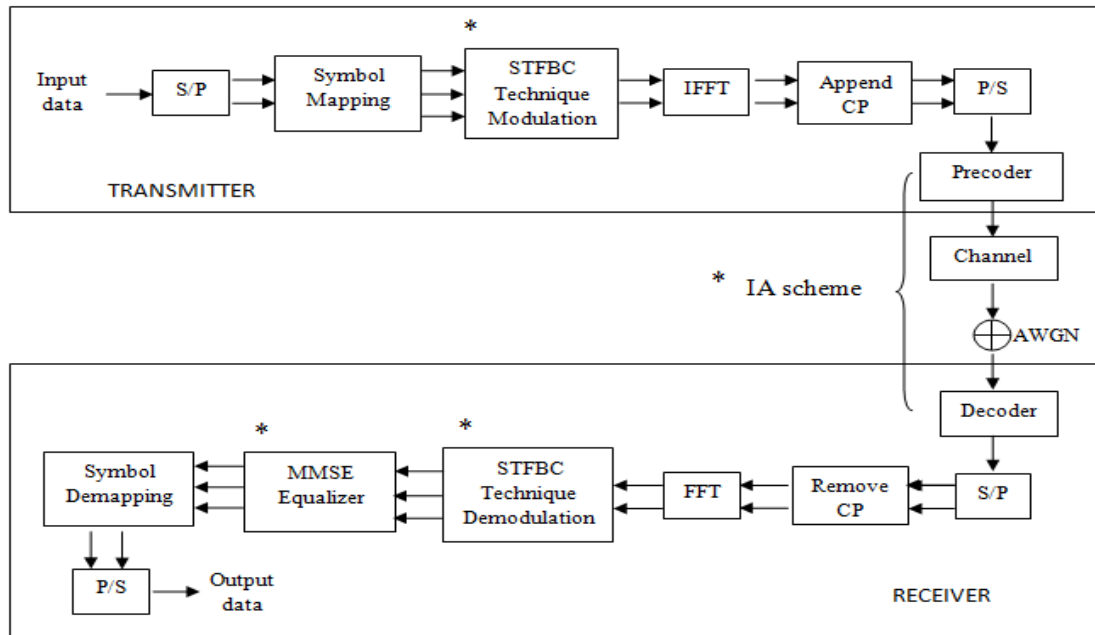


Fig.1 OFDMA system block diagram

After that, the data is converting back to the serial form before delivered to the precoder. At this stage, the linear precoding is being generated to perform interference alignment scheme before sending to the receiver. At the receiver, cyclic prefix is removed and N-point fast Fourier transform (FFT) is performed per receiver branch. Then, the digital demodulation and decoding through the implementation of equalizer is done. To get the original message information, the data words will then be multiplexed.

STFBC Technique

In the proposed system model, the Space Time Frequency Block (STFB) coding technique are used as it takes an advantage of diversity of space, time and frequency and hence can help to enhance the reliability and system performance. The coding distributes symbols along transmit antennas, time slot and OFDM sub channels. A STF codeword may occupy several OFDM symbols which can increase the diversity order [11] [12]. The coding of this technique is shown in Table 1.

Table 1. Space Time Frequency Block Codes Technique

Antenna time slot Frequency	Ant1 (T1)	Ant 2 (T2)
f1	X_k	X_{k+1}
f2	$-X_{k+1}^*$	X_k^*

The proposed technique is implemented by applying the interference alignment scheme (that will be discuss later) in a state of that the transmit symbol (independent codeword) is send by using the space time frequency block codes technique referring to table 1 above. In other word is that, sending the independent codeword at different time and frequency by using multiple antennas, so that, the system can exploit the space, time and frequency domains. It is happened since the STFB codeword may occupy several OFDM symbols and hence the diversity order can be increased. For example, based on table 1, the X_k is represented the first codeword that carries the first message of input vector that will be transmitted by transmit antenna 1 during the time slot 1 and frequency slot 1 followed by the second symbol X_{k+1} and so on.

Interference Alignment Scheme

Basically, in the MIMO channel the input output equation is given by

$$Y^{[1]} = H^{[11]}V^{[11]}X^{[11]} + H^{[11]}V^{[21]}X^{[21]} + H^{[12]}V^{[12]}X^{[12]} + H^{[12]}V^{[22]}X^{[22]} + N^{[1]} \quad (1)$$

$$Y^{[2]} = H^{[21]}V^{[11]}X^{[11]} + H^{[21]}V^{[21]}X^{[21]} + H^{[22]}V^{[12]}X^{[12]} + H^{[22]}V^{[22]}X^{[22]} + N^{[2]} \quad (2)$$

Where $Y^{[1]}$ is the $N_1 \times 1$ output vector at receiver 1, $Y^{[2]}$ is the $N_2 \times 1$ output vector at receiver 2, $N^{[1]}$ is the $N_1 \times 1$ additive white Gaussian noise (AWGN) vector at receiver 1, $N^{[2]}$ is the $N_2 \times 1$ AWGN vector at receiver 2. $X^{[1]}$ is the $M_1 \times 1$ input vector at transmitter 1, $X^{[2]}$ is the $M_2 \times 1$ input vector at transmitter 2, $H^{[11]}$ is the $N_1 \times M_1$ channel matrix between transmitter 1 and receiver 1, $H^{[22]}$ is the $N_1 \times M_1$ channel matrix between transmitter 2 and receiver 1, and $H^{[21]}$ is the $N_2 \times M_1$ channel matrix between transmitter 1 and receiver 2.

Hence, interference alignment refers to the careful choice of the vector directions in order to separate the desired signals at their respective receivers but the interference is aligned. For example, based on equation (1) for the receiver 1, the $H^{[11]}V^{[11]}X^{[11]}$ and $H^{[12]}V^{[12]}X^{[12]}$ occupy the same spatial dimension while the interference vectors $H^{[11]}V^{[21]}X^{[21]}$ and $H^{[12]}V^{[22]}X^{[22]}$ will share the same signal space.

MMSE Equalizer

On the other hand, the MMSE equalizer is chosen to be implemented in the receiver part of the system because based on the previous researcher, [5] they claimed that this type of equalizer is more balanced linear equalizer compared to the zero-forcing (ZF) and maximum likelihood sequence estimation (MLSE) equalizer.

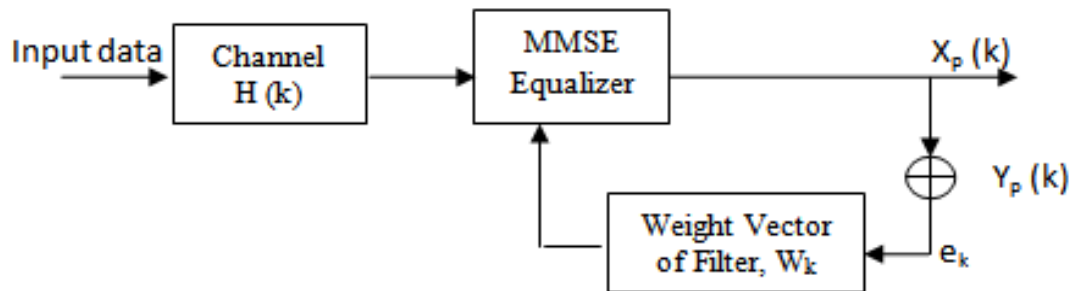


Fig. 2 Block diagram of MMSE Equalizer

Fig. 2 shows a block diagram whereby a few parameters involved which are, $H(k)$ is the channel impulse response, $X_p(k)$ is the actual output while the $Y_p(k)$ is the desired output. The e_k is the error between these two output of the system. In this type of equalizer, the tap weights are chosen as they minimize the mean-square-error (MSE) of all the ISI terms and the noise power at the output of the equalizer. MMSE is the expected value of the squared difference between the desired data symbol and the estimated data symbol. Error between desired and actual output is given by [10]

$$e_k = x_p(k) - Y_p(k)^T W_k \quad (3)$$

where W_k is the weight vector of filter. Mean square error is the square of Equation (3) which produces Equation as followed,

$$MSE = E[X_p(k)]^2 + W_k R W_k - 2P^T W_k \quad (4)$$

R and P are the correlation and auto-correlation matrices. To minimize ISI we have to find filter weights which minimized when $R = P W_k$. The vector W_k corresponds to the number of taps in the equalizing filter. The equalizer correction term which is the inverse of channel response multiplying with the received signal produces the equalizer output as below,

$$C_{MMSE} = \frac{1}{[H(k)+N]} \quad (5)$$

where the $H(k)$ is the channel impulse response, while the N is the noise in the system.

RESULTS AND DISCUSSION

STBC,SFBC and STFBC Technique

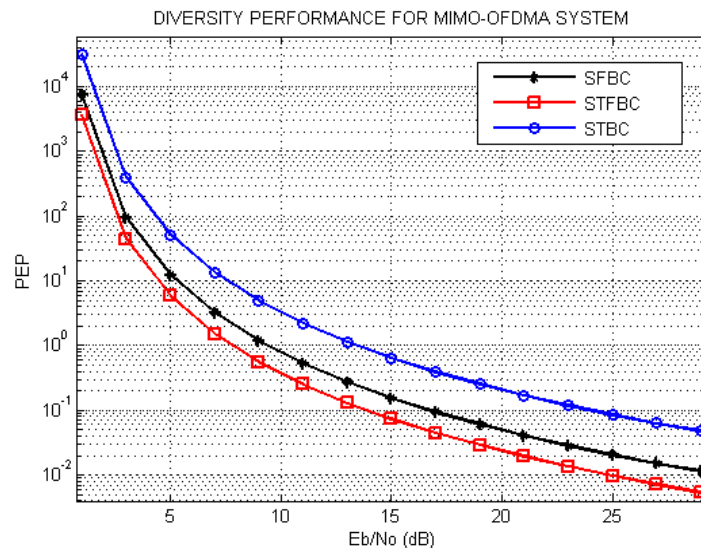


Fig. 3 PEP performance between three different diversity techniques

Fig. 3 shows the PEP performance comparison between diversity order systems. Space time frequency diversity (STF) offers the higher diversity order compared to space time (ST) diversity and space frequency (SF) diversity because it exploits the time and frequency slot during transmission of data through different antennas. From the simulation result, at $E_b/N_0=25\text{dB}$, STFBC is 9×10^{-3} , achieves the smallest value of PEP indicates the smallest amount of interference in the system, compared to the SFBC and STBC which is get the PEP value of 2×10^{-2} and 8×10^{-2} respectively. Hence, it is prove that the performance of the system is improve by using the STFBC technique as the SNR is increased while interference and PEP value is decreased.

Performance of IA scheme

Fig. 4 shows the PEP performance comparison of IA scheme between three different conditions. IA scheme is able to reduce the interference in the system by achieving the PEP value of 1.8×10^{-5} at $E_b/N_0=25\text{ dB}$. Then, it is being improved when the IA is applied by using the STFBC transmission method, getting 1.3×10^{-5} value of PEP. This is because; in this condition, by using the STF block codes, the data is able to be transmitted at different antenna, time and frequency domain throughout the system. Moreover, the system is further improved when implementing the MMSE Equalizer together with the STFBC-IA technique. This is happen as equalizer has the ability to reduce the ISI in the system. Hence, the SNR is increased while PEP and interference is decreased. It is proves that the combination of three different method of STFBC-IA-MMSE gives the best performance and outperforms the other two condition method by producing the 6×10^{-6} of PEP value, hence giving about 66.67% improvement compared to the system with IA scheme only.

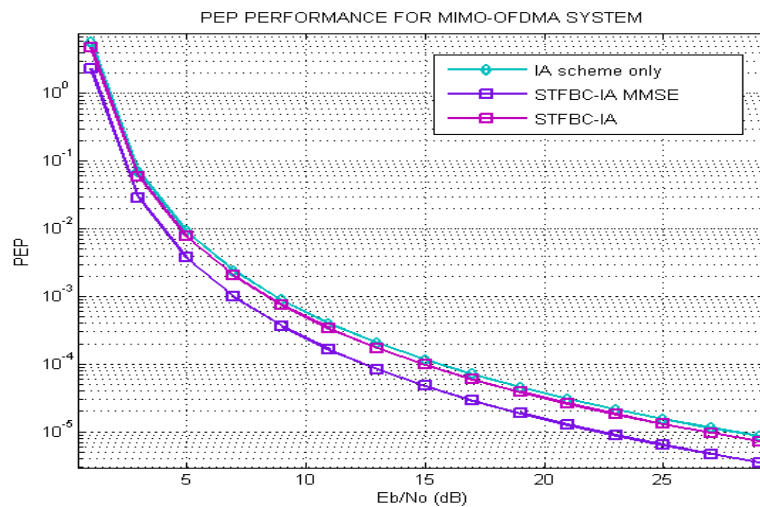


Fig. 4 PEP performance of IA scheme

CONCLUSION

IA scheme is applied in the system in order to reduce the ICI. This IA scheme is improved by applying the STFBC technique modulation and giving about 70% improvement. Besides, ISI is also emerging in the system due to the multipath propagation that causes fading of received signal power. The equalizer is believed to be able to improve the distorted received signal caused by ISI. So, the MMSE is chosen to be implemented in order to solve this matter and improved about 58% compared to the system with STFBC-IA scheme only. From the simulation results, it can be proved that with the implementation of STFBC-IA-MMSE, the ISI and ICI can be mitigated, and also higher diversity order is achieved, hence improved the PEP system performance. This is meets the objective of presented study.

REFERENCES

- [1] Morelli. M., Kuo. C. and Pun M. (2007). Synchronization techniques for orthogonal frequency division multiple access (OFDMA): A tutorial review, *PROCEEDINGS-IEEE*. **95**(7): 1394-1427.
- [2] Xu J., Kim J., Paik W., and Seo J. (2006). Adaptive Resource Allocation Algorithm with Fairness for MIMO-OFDMA System. *IEEE Transactions on Wireless Communications*. **00**: 0-4.
- [3] Zheng, L. and Tse, D.N.C (2003) Diversity and Multiplexing: A fundamental tradeoff in multiple-antenna channels. *IEEE Transactions on Information Theory*. **49**(5): 1073–1096
- [4] Aziz, B., Fijalkow, I. and Ariaudo, M., (2010) Intercarrier interference in uplink OFDMA systems with carrier frequency offset. *21st Annual IEEE International Symposium on Personal, Indoor and Mobile Radio Communications*, pp. 746–751, Sep. 2010.

- [5] Idris, A., Abdullah, N., and Hussein, N.A. (2014). Optimization of BER Performance in the MIMO-OFDMA System for Mobile WiMAX System using Different Equalization Algorithm. *ARPJ Journal of Engineering and Applied Sciences*. 9(8): 1177–1182.
- [6] Idris, A., and Dimyati, K. (2008). Performance Evaluation of Inter-carrier Interference Self-Cancellation Schemes for Space Time Frequency Block Codes MIMO-OFDM system., pp. 1–5.
- [7] Tresch, R. and Guillaud, M., (2009). Cellular interference alignment with imperfect channel knowledge. In *Communications Workshops, 2009. ICC Workshops 2009. IEEE International Conference on*, pp. 1-5.
- [8] Shen, H., Li, B., Tao, M. and Luo, Y., (2010) The new interference alignment scheme for the MIMO interference channel. In *Wireless Communications and Networking Conference (WCNC), 2010 IEEE*, pp. 1-6.
- [9] Idris, A., Abdullah, N., Ali, D.M., Ya'acob, N. and Mohamad, H.A., (2013). Reduction of interference with linear equalizer using quarter subcarrier mapping scheme. In *Wireless Technology and Applications (ISWTA), 2013 IEEE Symposium on*, pp. 57-61.
- [10] Gupta, B. and Saini, D.S., (2010). BER performance improvement in OFDM systems using equalization algorithms. In *Parallel Distributed and Grid Computing (PDGC), 2010 1st International Conference on*, pp. 49-54.
- [11] Liu, Z., Xin, Y. and Giannakis, G.B., (2002). Space-time-frequency coded OFDM over frequency-selective fading channels. *IEEE Transactions on Signal Processing*, **50**(10): 2465-2476.
- [12] Fitz, M.P., Grimm, J. and Siwamogsatham, S., (1999). A new view of performance analysis techniques in correlated Rayleigh fading. In *Wireless Communications and Networking Conference, 1999. WCNC. 1999 IEEE*, **1**: 139-144.
- [13] Su, W., Safar, Z. and Liu, K.R., (2005). Towards maximum achievable diversity in space, time, and frequency: performance analysis and code design. *IEEE Transactions on Wireless Communications*, **4**(4): 1847-1857.

Livestock Information System using Android based Architecture

M.H. Ariff¹, I. Ismarani², N. Shamsuddin³

¹Faculty of Electrical Engineering, Universiti Malaysia Pahang, 26600 Pekan, Pahang, Malaysia.

²Faculty of Electrical Engineering, Universiti Teknologi MARA, 40000, Shah Alam, Selangor, Malaysia.

³Standards and Industrial Research Institute of Malaysia, 57000, Bukit Jalil, Kuala Lumpur, Malaysia.

(*corresponding author email: hisyam@ump.edu.my)

Received: 27.08.2015; accepted: 30.10.2015

Abstract These days most of livestock breeders have tried many new methods to ensure their livestock in good condition and profitable through the sale of their livestock. Failure to ensure the health of livestock can pose a danger to a consumer because of the livestock diseases such as mad cow disease can cause harm to humans. Traditional techniques by using manpower to observe of livestock monitoring will result in wastage of manpower and time. In addition, the use of old methods such as pencil and paper to record information of livestock data is unsafe, often occurs human error in recording and impractical. Thereby, the use of electronic methods in livestock monitoring will facilitate the effective way of storing the livestock profile. In this project, the use of Android smartphone as host to display result, RFID in creates a livestock's profile and also some sensor equipment for weight and body temperature has provide efficient and fast method to facilitate the parties involved in the livestock industry, such as farmer, veterinary expert or any interested parties to share information livestock through electronic storage such as server and cloud storage platform.

Keywords RFID – sensor – livestock – animal identification – agriculture

INTRODUCTION

For some decades, agriculture has been associated with livestock production and crops to provide an important food source for humans. At present, agriculture has entered a new phase which includes forestry, cultivation of fruits, dairy products, bee keeping, mushroom and many others. In addition, today the process of production, marketing and distribution of livestock and crops recognized as part of the current agriculture. Agricultural component plays an important role in contributing economic profit of a given country [1-2]. Furthermore, creating a raw material for food provides an employment to a very large percentage of the population in the world. Globally, animal identification is a huge market across the countries and has a potential rate exceeding 30 percent per year [3]. Millions of cattle, birds and pet are identified and tracked using electronic identification technologies, primarily Radio Frequency Identification (RFID) technology. Previously, bar-codes were used for animal ID,

which is now rapidly being changed by RFID because of the latter's advanced advantages and features. RFID does not require a line-of-sight between the tags and the readers [4]. A reader can read RFID tags from a distance. As a result, with anti-collision technology, a reader can read multiple tags at a time thus tracking and identifying several animals at the same time. This not just ensures safety and security of the animals, but also reduces the requirement of manual labour and the time taken to identify the animals.

The awareness of the importance of using International Standards Organization, ISO 11784, ISO 11785 and ISO 14223 for animal identification are still low especially on developing countries. In contrast, countries such as Europe, Australia and Canada starts to implement this system [5-7]. As a direct result of this adoption, any livestock producers wishing to export animal to these countries must have proper identification and tracking records which mandate the use of RFID. Using the unique numbered RFID tag provides a very fast technique of identifying animals and collecting data more efficiently. Each unique RFID tag can be linked to the database.

Nowadays, compact and small wearable sensors have become widely available, which allows convenient and practically monitoring of the weighing scale and temperature for animal monitoring purposes [8-10]. In addition, globally, the existence of many smart phones comes with extra features such as web browsing, internal memory, thumb recognition, local wireless area networks (Wi-Fi) and the Internet [11-12]. This makes newer smart phones a very compromising mobile architecture to create advanced applications. In order to complete the trends, the popular data storage platform with security and privacy features such as Google Drive and Dropbox are observed. The advantages of Google Drive includes, it links information between disease infected animals and multiple veterinary experts. Beyond that, it also maintains the data of animal profiling report and provides easy access to the Livestock's own records from any locations. Finally all the important parameters for livestock data also can be exports to the third-party laboratory for further analysis purposes. Thus, it is good to bring wearable sensors with smart phones, Bluetooth and Google Drive together to create a personalized, integrated, and collaborative livestock monitoring system for real time, long term and remote monitoring the additional data extracted from flock book such as medication, animal profile, group and farm movement.

DESIGN ARCHITECTURE FOR A LIVESTOCK MONITORING SYSTEM

System Architecture Structure

The Livestock monitoring system that was built for this project consists of several basic components of RFID technologies such as RFID portable reader and RFID tag technology in order to collect information on livestock profiling at the entrance of the barn. The information gathered from RFID portable reader can be transferred to the android smartphone that act as a host via Bluetooth connection between this devices. Furthermore, livestock information also can be transferred to the central server that receiving and managing data transmitted from smartphone and supports connections with interested clients. As a result, third parties user that communicate with the server via TCP / IP, Google Drive can alert the symptoms of the selected livestock when it was examined as shown in Fig.1. The sensor part, which

measures livestock's temperature information, is composed of sensors that could measure the livestock body core temperature and weight through them in real time and converts the measured livestock information into a suitable form of signal processing to send it to smartphone.

The smartphone that collecting the livestock's profiling from a scheduled test for the livestock able to store data in memory phone and further send it to the server via the gateway.

The gateway is functioning to maintain and create a network of sensor point to collect unique information of livestock. Furthermore, gateway also provide a structural communication with the central server and perform the function of collecting RFID unique ID and data of livestock information collected from the sensor point to deliver it to the central server.

The central server activates the real-time livestock monitoring system, then registers information of the gateway and sensor point according to the network built by the gateway, stores livestock's information and data information sent from the sensor nodes into a database and maintains it. In addition, it provides livestock's profiling information through mobile clients in real time.

A mobile client is comprised of application services supporting the mobile platform, and provides a livestock monitoring service and livestock's dangerous situation notification service *etc.*, to users via the management server and TCP/IP communications.

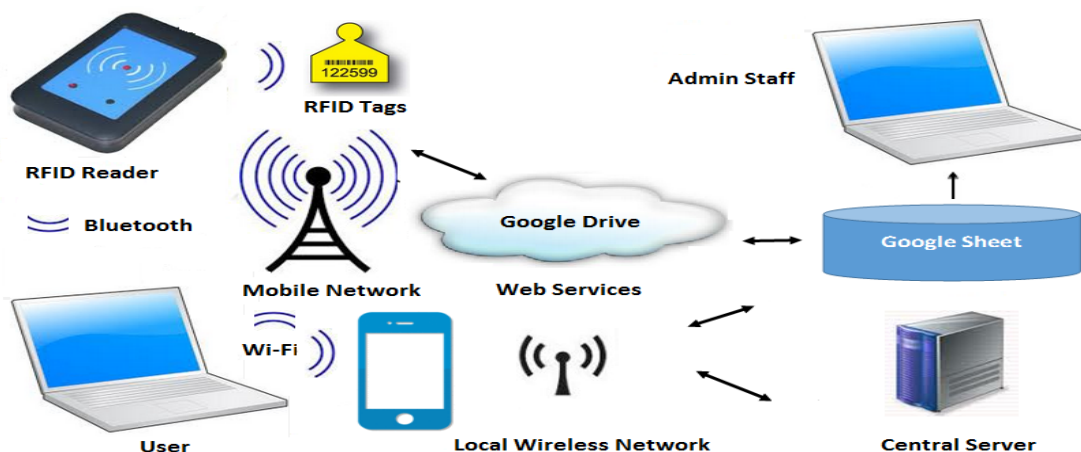


Figure 1. The structure of the proposed livestock monitoring system.

Class Diagram

A class diagram identifies classes, relationships between attributes, methods and attributes. In this livestock monitoring project, class diagram is used as a basis to develop other Unified Modelling Language (UML) diagram including collaboration and sequence diagram. The proposed system provides users with the livestock monitoring service with which they can monitor the livestock information and livestock barn environment information, the livestock barn facility control service for optimal management of livestock breeding environment, and

livestock's dangerous situation notification service to inform a danger of the livestock when emergency situation occurred.

Livestock Monitoring Class Diagram Service

The livestock monitoring service is a service which enables livestock producers to monitor through a GUI important animal profiling information such as sex, date of birth, farm location, status of livestock, breed, name of breeder which were manually inserted by users and sensor data such as livestock's temperature, livestock's weight and information of the livestock barn. Fig. 2 shows operation process of the livestock monitoring classes designed for Android OS.

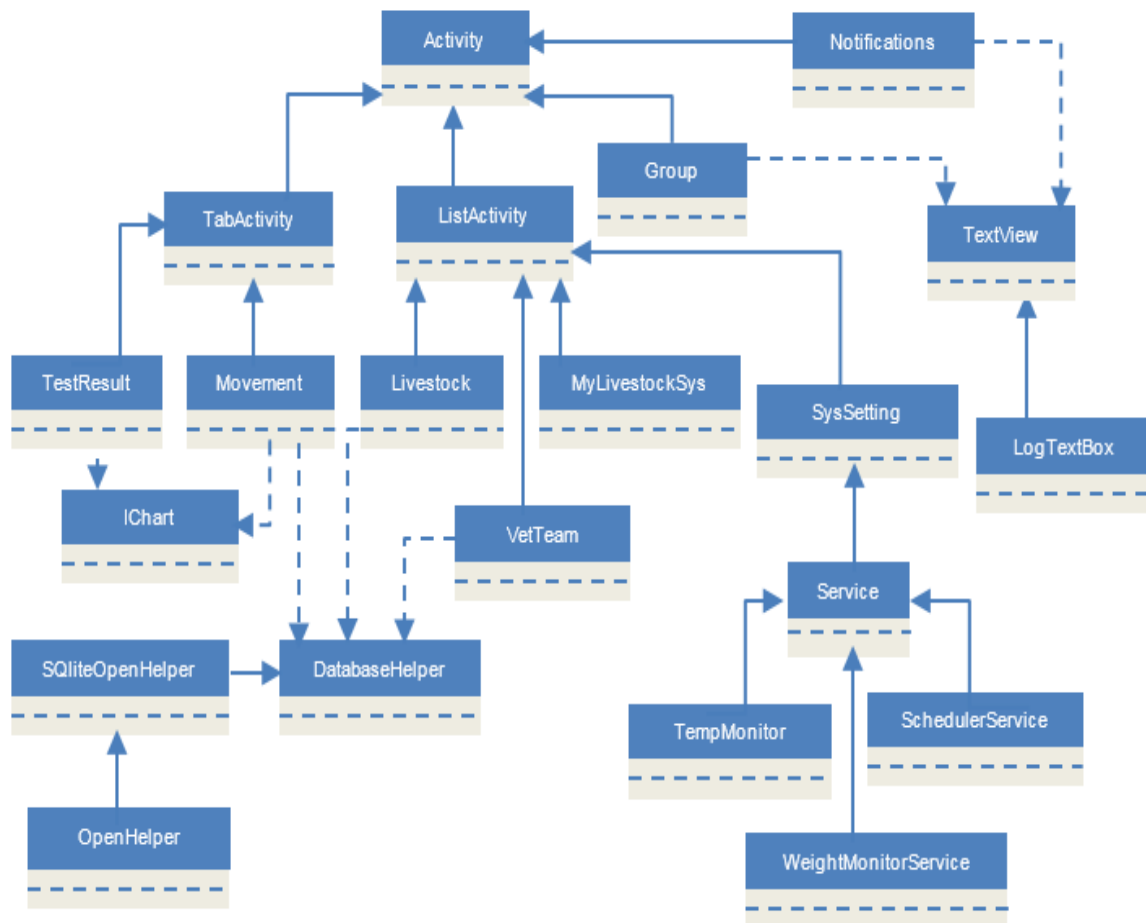


Figure 2. Class overview of the livestock monitoring service.

Software and Hardware

In developing the livestock information hardware system, some sensors have been used mainly to meet the two groups of livestock health data collection such as Core Body Temperature and weighing measurement. In addition all the sensor data can be obtained from the sensors and processed in our own sensor network. Table 1 shows hardware development for sensory devices.

Table 1. Hardware Development for Sensory Devices.

Measuring Sensor	Model	Manufacturer
BodyCore Temperature	Fever Tags	Fever Tag LLC
Weighing Measurement	Cattle Weight	Commander AG- Quip
Livestock Id	UHF RFID Tag SH- I0701	Shenghua

Fever Tags was used to measure the livestock's temperature which is a tympanic thermometer device pinned to the ear with a probe inserted in the lower ear canal. This device flashes an indicator light when the temperature is greater than a set temperature such as 55°C.

Cattle Weight device was used to measure the livestock weight. Livestock owners often need to know the weight of their animals in order to determine proper feed rations, to administer the proper dosage of a medication, or to track how individual animals grow and use their feed.

Finally, for livestock identification, Shenghua UHF RFID animal ear tags are used for livestock information system. It's made of polymer materials, non-toxic and does not affect raising the animals. The main reason of using UHF frequency tags is because it gives large better read range which typically from 3m to 10m depends on reader's antenna. The operating frequency for this passive tag are in the range of 860 MHz to 960MHz and adequate for global use. In addition, this tag meets the EPC C1G2 / ISO 18000-6C standards.

The following tools are used through this project to build, test and analyze the livestock parameters as shows in Table 2.

EXPERIMENTAL WORK ON LIVESTOCK MONITORING SYSTEM.

The performance of this livestock health system was tested on the livestock farming owned by Malaysian Agriculture Research and Development Institute (MARDI) located in Kemaman, Terengganu. Fig.3 shows the experimental work on the farm field.

Before the UHF tag attached to the ears of cattle, all the tags have been divided into two groups for the use of bulls and heifers which each group received 25 tags. The first test was to insert four UHF readers in the central server and the related information of the barn. It was found that the system entered the several readers correctly and could establish a connection with all of them successfully. The second test consisted of simultaneously placing several tags in the reading range of one reader to see if the system could record all accesses. It was found that even when three tags were placed at the same second, the system was able to record the livestock.

Table 2. Software Development.

Software Tool	Function
Android Software Development Kit (SDK)	Provide the user with sample project, an emulator, and development tools. In this project API level 10 is used.
Eclipse and Android Developer Tools plug-in (ADT)	Create an application UI, add components based on the Android Framework API and debug applications. In this project Eclipse Kepler version 4.3.1 is used.
Dalvik Debug Monitoring Service (DMMS)	Debugging interface between the application and the IDE.
Java Development Kit (JDK)	Program platform since this Android Applications are program in Java. In this project, JDK 7 was used.
Android Debug Bridge (ADB)	Tool that manage either an emulator instance or an actual Android powered device.

Another test was that the system only registered one cattle from each barn, regardless of the time that tag being scan by the farmer. Several tags were placed near all readers at the same time, hence all cattle tags were registered on the central server successfully.

**Figure 3.** Experimental work on livestock farm field.

RESULTS AND DISCUSSION

Based on Livestock system architecture, a prototype system consist of the following important component was developed where the monitoring algorithm can be applied on the different operating systems such as Windows, Linux or Android. Table 3 shows the summary of main menu and its function.

Table 3. Summary of Main Menu and Its Function.

Menu	Function
Veterinary Term	Display the health care team information such as name, phone number, email address and address of animal health care centre.
Livestock	Contains record of animals such as sex, date of birth, farm location, status of the livestock, breed, name of breeder, date of infection and date of disinfections.
Groups	Contains summary of information on group animals on the farms such as cattle and sheep.
Movements	Contains the information of the livestock movement such as source location and transfer new location.
Test Results	Contains progress report (body temperature and weight) of animal's health graphs in daily, weekly or monthly.
Medications	Contains name and quantity of the medicines given to the livestock. In addition name of caretakers also includes in this menu.
Report Data	Contains specific information of the livestock that can be send to stockman, breeder, buyer and DVS.
Setting	Setting the connection of RFID reader.

Fig.4 shows the real Graphical User Interface for Livestock Information System appears in actual smartphone. Fig.5 shows the extra features of this menu is that users can send report data to the other interested third party such as stockman, breeder, buyer and department of veterinary services through the internet cloud storage such as Google Drive. Moreover, this livestock information can be shared everywhere in the world at any time if using this services. On the capability of display of information for sensory devices, the livestock system described in Fig. 6 do a complete generation for information regarding to the livestock temperature. In addition the first case on the database that issued the temperature and in the

second case on the database of a particular weight in which animal profiles must be registered in this system. This approach, it is only in the livestock farm facilities where livestock have been doing medical examination that the system runs a query, resulting in improved general efficiency of the system.

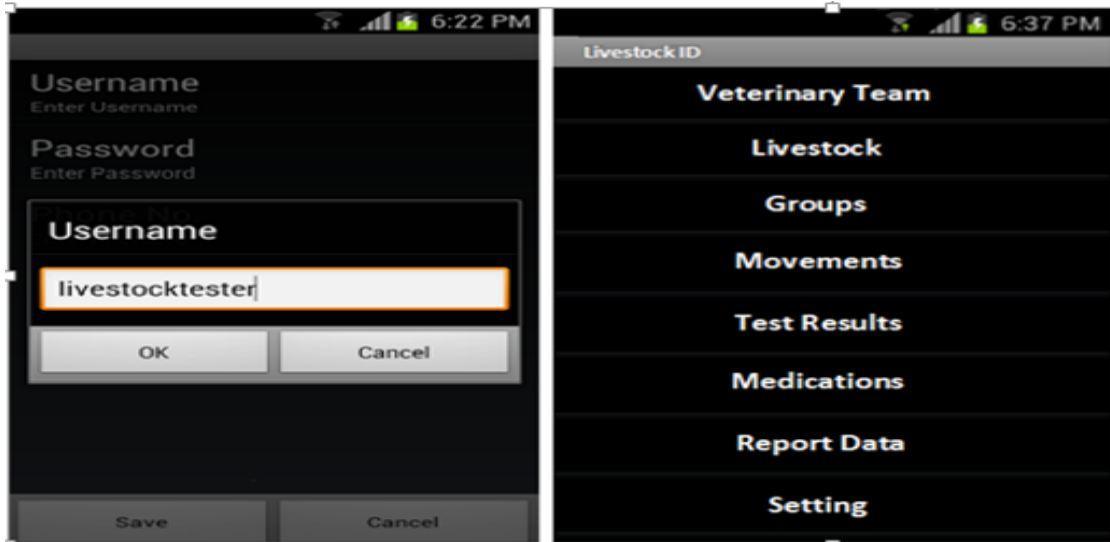


Figure 4. Graphical user interface for livestock information system.

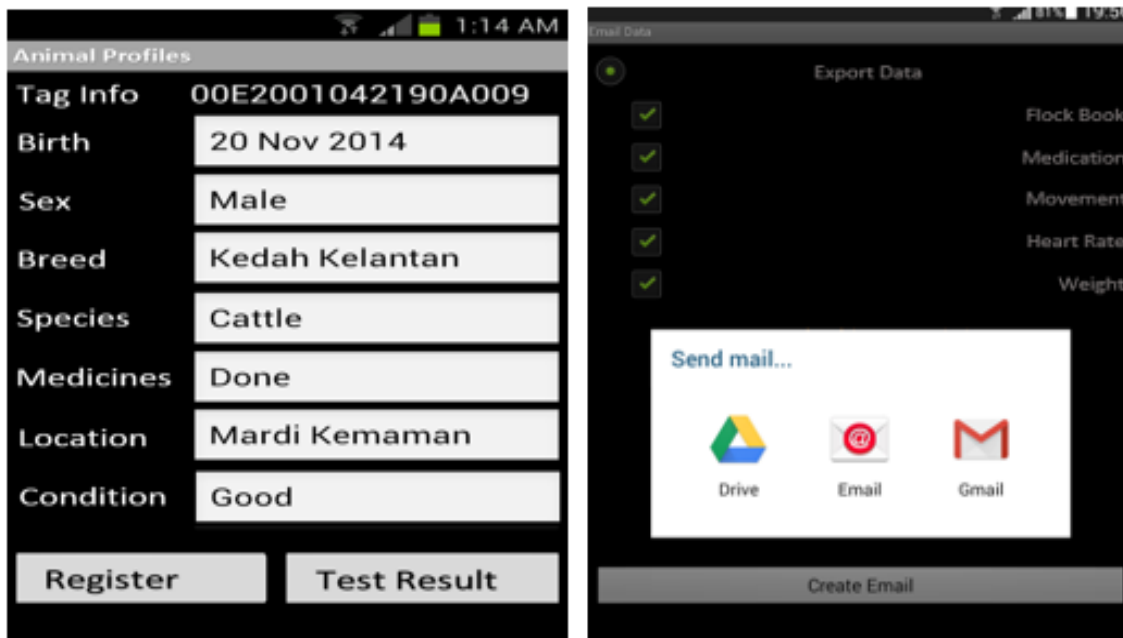


Figure 5. GUI of the Tag registration and Storing Process.

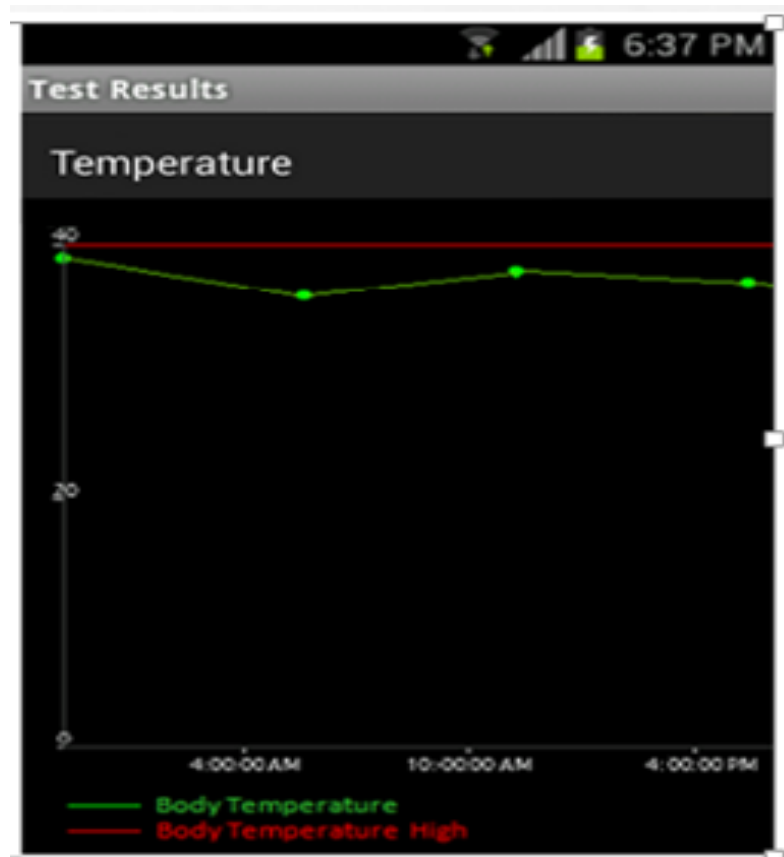


Figure 6. GUI of livestock health record.

FLOCKBOOK							
No	Tag	Management Tag	Date of Birth	Species	Status	Sex	
1	0000AD000013070200575211	2012102001	20-Oct-12	Cattle	Available	Male	
2	AD291500185B65806900008A	2012101501	15-Oct-12	Cattle	Available	Male	
3	AD2A16004245B18B4A0000C9	2012082101	21-Aug-12	Cattle	Available	Male	
4	AD2B300041BFF5803E000026	2012070501	05-Jul-12	Cattle	Available	Female	
5	E20068060000000000000000	2012060401	04-Jun-12	Cattle	Available	Female	
6	E28068100000003900C6F677	2012040101	01-Apr-12	Cattle	Available	Female	
7	E2806E8F000000390060D0DD	2012032101	21-Mar-12	Cattle	Available	Female	
MEDICATION							
Med Id	Medicine Type	Batch Number	Expiry Date	Admin Date	Administrator	Amount	Unit
5790	Penicilin 250 mg	20120602	20-Oct-12	19-Feb-14	Researcher	30 ml	
5791	Penicilin 250 mg	20120602	20-Oct-12	19-Feb-14	Researcher	30 ml	
5792	Penicilin 250 mg	20120602	20-Oct-12	19-Feb-14	Researcher	30 ml	

Figure 7. Report generated in Excel format.

A livestock's medical history is very important for veterinary expert in the process determination and diagnose of the suitable treatment for the livestock. In emergency cases, when these operations must be carried out in limited time, fast retrieval of profiling related to livestock's medical history may be of vital importance for the livestock's life. In this project, the report can be generated in the form Excel format and can printed out in the form of paper sheets. Fig. 7 shows the report generated in Excel format.

CONCLUSION

In this paper "Livestock Information using Android Based Architecture" has been presented to determine the health status of the livestock. All the research element and embodiment of this mobile livestock information system care device are described. The device powered by Android operating system provides some information of temperature for the livestock and medication taken by the livestock. This device integrates several features and functions that make it prominent form others. In most products, determination of livestock information system will be based on manual flock book and some of the device required complicated setting before doing the measurement. This system is reliable, user friendly and can be used in the field for a long time since the system generates power from mobile battery system.

Acknowledgments

This research is supported by Malaysian Ministry of Science, Technology and Innovation Grant 100-RMI/SF 16/6/2 (5/2013). The authors would like to thank Universiti Teknologi MARA and SIRIM Berhad for providing the facilities to conduct this research and for financial supports throughout the process.

REFERENCES

1. Lemaire, G., Franzluebbbers, A., de Faccio Carvalho, P. C., & Dedieu, B. (2014). Integrated crop–livestock systems: Strategies to achieve synergy between agricultural production and environmental quality. *Agriculture, Ecosystems & Environment*, 190, 4-8.
2. Young, J. R., Rast, L., Suon, S., Bush, R. D., Henry, L. A., & Windsor, P. A. (2014). The impact of best practice health and husbandry interventions on smallholder cattle productivity in southern Cambodia. *Animal Production Science*, 54(5), 629-637.
3. Masiga, W. N., & Munyua, S. J. M. (2014). Global perspectives on animal welfare: Africa. *Revue scientifique et technique-Office international des épizooties*, 24(2).
4. P.J. and I. Sweeney (2005). RFID for Dummies: Wiley Publishing, Inc.
5. V. Chawla and D. S. Ha (2007). "An overview of passive RFID," *Communications Magazine, IEEE*, vol. 45, pp. 11-17.
6. H. Knospe and H. Pohl (2004). "RFID security," *Information Security Technical Report*, vol. 9, pp. 39-50.
7. O. Ribó, C. Korn, U. Meloni, M. Cropper, P. De Winne, and M. Cuypers (2001). "IDEA: a large-scale project on electronic identification of livestock," *Revue Scientifique et Technique-Office International des Epizooties*, vol. 20, pp. 426-433.

8. Ariff, M. H., Ismarani, I., & Shamsuddin, N. (2014). RFID based systematic livestock health management system. *2014 IEEE Conference on Systems, Process and Control (ICSPC)*, pp. 111-116.
9. M. Radenkovic, B. Wietrzyk (2006). "Wireless Mobile Ad-Hoc Sensor Networks for Very Large Scale Cattle Monitoring", *In Proc. Of Sixth International Workshop on Applications and Services in Wireless Networks (ASWN'06)*, Berlin, Germany, pp.47-58.
10. H. Agematsu, J. Kani, K. Nasaka, H. Kawabata, T. Isohara, K. Takemori, and M. Nishigaki (2012). "A Proposal to Realize the Provision of Secure Android Applications -- ADMS: An Application Development and Management System," *2012 Sixth International Conference on Innovative Mobile and Internet Services in Ubiquitous Computing*, no. i, pp. 677–682.
11. Erika Chin, Adrienne Porter Felt, Kate Greenwood, David Wagner (2011). "Analyzing inter-application communication in Android", *Proceedings of the 9th international conference on mobile systems, applications, and services*, NY USA.
12. G. Chang, C. Tan, G. Li, and C. Zhu (2010), "Developing mobile applications on the Android platform," in *Mobile multimedia processing*, ed: Springer, pp. 264-286.

Differentiating Ischemic Stroke Severity Using Artificial Neural Network

Omar WRW¹, Mohamad Z², Taib MN³, Jailani R⁴

^{1,2}Department of Electrical Engineering, Politeknik Sultan Salahuddin Abdul Aziz Shah, 40150 Selangor, Malaysia.

^{1,3,4}Faculty of Electrical Engineering, Universiti Teknologi MARA, 40450 Selangor, Malaysia.

(*corresponding Author: rosemehah@yahoo.com)

Received: 30.09.2015 ; accepted: 09.11.2015

Abstract Stroke or cerebrovascular accident (CVA) or angin ahmar in Malay language is one of the major burdens to the Malaysian healthcare system due to the increase in the number of stroke victims. The Disease Burden Study indicated that stroke is ranked third behind ischemic heart disease and mental illness. As part of an on-going research in grouping the stroke level, the application of Artificial Neural Network (ANN) is proposed in this study to analyze brainwave using EEG. The work involves of selected stroke subject from Advance Group (AG) Intermediate Group (IG) and Early Group (EG), the features extraction of brainwaves using Relative Power Ratio (RPR) to identify the significant brainwave as input to the network. The ANN programming algorithm was developed and computed automatically via Matlab software version R2010b. Levenberg Marquardt (LM) training algorithm and sigmoid transfer function were used to optimize the parameters in the training network. The result obtained showed the capability of ANN in analyzing the stroke severity hence beneficial for the further application such as grouping and classification for stroke severity based on the brainwave behaviour of the ischemic stroke patient.

Keywords Stroke; Electroencephalogram (EEG); Artificial Neural Network (ANN).

INTRODUCTION

ANN is a data processing technique or algorithm that operating as human brain to activate the signals for processing. The properties of ANN that demonstrate brain like behavior has made it possible to be applied in many different field in order to tackle problems that were considered to be very difficult or unsolved. Nowadays, ANN models are the subject of study in many areas including system identification and control such as in plantation [1] and [2], fragrance industry [3], medical [4], sequence recognition such as face, speech, handwritten text recognition [5],[6],[7] and data mining or knowledge discovery in databases [8].

The ANN training requires very long task. It requires several repeated training sessions followed by an exhaustive process evaluation in order to select the training with the best result [9]. The ANN training can be categorized into two categories supervised and unsupervised learning. Supervised learning uses pattern classifier to relate specific class to specific sensor output while unsupervised learning does not require predetermined classes for training [10]. In order to achieve some applications such as pattern recognition, classification, prediction and controlling, the network functioning based on biological neural

system. This highly parallel interconnected system is built by neurons or nodes which are connected together [11].

This research mainly observes the behaviour and characteristic of ischemic stroke brainwave signals. Such finding is being developed as a model through techniques like ANN. Many applications of ANN has been found in the fields of biomedical system for prediction, prognosis and diagnosis such as prognosis of dengue fever[12], cancer detection [13], and modelling of heart disease recognition [14]. Therefore, as part of an on-going research in grouping the severity of ischemic stroke, the application of ANN is proposed to analyze severity of ischemic stroke using the brainwave signals. The brainwave signals are refer to the significant brainwave pattern in signal processing that influence the behavior of ischemic stroke patient.

METHODOLOGY

This part explains extensively on the processes that have been implemented for this research work.

Data collection

The EEG measurements were carried out at NASAM, Petaling Jaya, Selangor, Malaysia. The stroke patients were grouped into three severities depending for their progression score. There are advance group (AG), intermediate group (IG) and early group (EG). The patients will undergo several physical assessment carried out by NASAM to classify them into these three groups of stroke severity. The subjects are categorical base on their dependency on staffs for carrying out their activities. Those who rely on staff to help them in 25% of their activities will be under AG. Those who require 25% to 75% of help will be under IG and those require more than 75% will be put under EG. Usually, those subjects under EG are wheel chaired. In this case, the stroke patients are classified by the physiotherapist at NASAM [15].

Signal Transformation

The signal transformation is carried out to extract the information from the gather results for data analysis. A vital step that must be taken into consideration for data analysis and pre-processing is artifact removal. The undesirable signals interfere with the neurological effect such as Electrooculography (EOG) and Electromyography (EMG) because of eye movements and muscle movements respectively [16, 17].

Power Spectral Density (PSD) is a very useful tool to identify signals in time series data and want to know amplitude. It is intended for continuous spectra, which has dimensions of power per hertz (Hz), helps identify periodicities describes how the power a signal or time series is distributed over the different frequencies. The unit of PSD is energy per frequency (width) that obtained energy within a specific frequency range by integrating PSD within that frequency range. Computation of PSD is done directly by the method called FFT. PSD refer to the specific to each frequency band and maximum energy power spectrum density. It is capable to capturing the maximum frequency content of stochastic process and can be calculated using periodic. This process is important to improve the accuracy and efficiency of data analysis in neural networks.

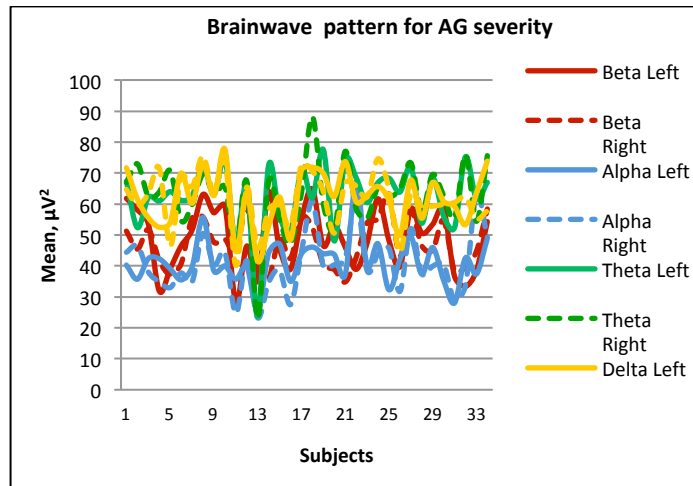
ANN structure and training

The main part in this research is ANN classification, which will be explained on the technique to predict and classify the corresponding stroke severity. Multilayer feed forward network will be implemented to classify stroke severity between AG, IG and EG with a value for classification bands setting is 1, 2 and 3 respectively. Firstly, the multilayer feed forward network models have been developed using input and target from stroke severity dataset, which is known as supervised learning. The methods for testing a model are concerned with analysing the model fit by calculate the Mean Squared Error (MSE). Base on the ANN modeling, the predictor values, y_{predict} have been recognize in a specific range of threshold for each group of stroke severity. The threshold is setting by observing the distribution of predicted group of stroke severity value. The same threshold is implemented to the ANN classification using the testing data.

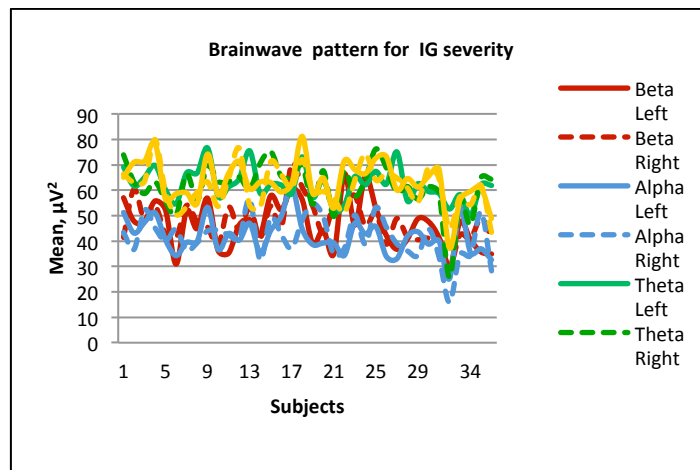
RESULTS AND DISCUSSION

Figure 1 (a), (b) and (c) shows the characteristics for each sub bands data plot for the Beta, Alpha, Theta and Delta power for left and right stroke patient for AG, IG and EG respectively after extracted the PSD data set. From this plot, each level is inconsistency range of power. It is notices that the electrical activity of a brain measured by EEG exhibits complex behavior and form of EEG sub bands patterns with different complexities value. However, it shows variation of pattern belongs to each of every sub band for each subject.

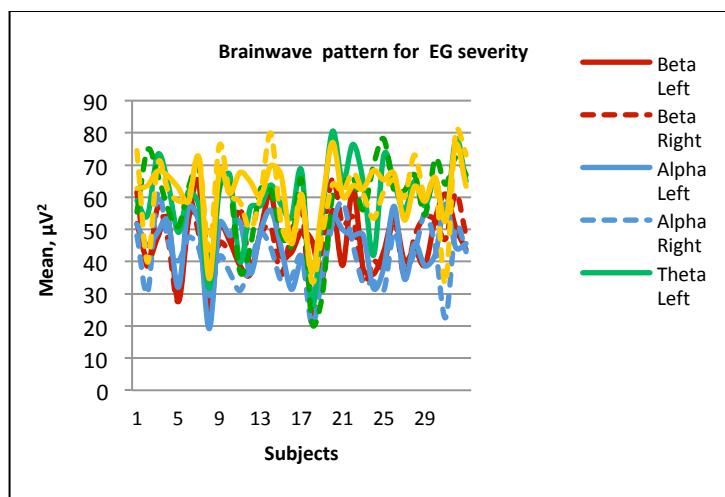
Table 1 shown the maximum and minimum power of EEG signals observe from Figure 1. The power of the signals varies according to the behavior of severity. For beta wave AG and EG are at the same behavior or state, whereas IG and EG are at the same state for Alpha and AG & IG are at the same state for Theta. The highest power is AG stroke severity for Delta wave ($88\mu\text{V}^2$ - $23\mu\text{V}^2$), and the lowest power ($70\mu\text{V}^2$ - $19\mu\text{V}^2$) is Alpha wave. Therefore, the range power would indicate the stroke severity. Thus, the uniqueness of the ischemic stroke EEG signal can contribute to the understanding the EEG brain processes and an innovative motivation for further analysis.



(a)



(b)



(c)

Figure 1. Beta, Alpha, Theta and Delta band power data plot for left and right for (a) AG subjects, (b) IG subjects and (c) EG subjects

Table 1. Maximum and Minimum Power of EEG from Ischemic Stroke Severity

severity	Beta (μV^2)	Alpha (μV^2)	Theta (μV^2)	Delta (μV^2)
AG	64-28	65-23	77-23	88-23
IG	70-30	61-16	77-25	81-68
EG	64-19	61-19	80-21	80-33
Max &min	70-19	65-16	80-21	88-23

Figure 2 depicts the ANN final training errors with varying hidden layer size. The hidden layer size is varies from 1 to 25. Graphically, it can be seen that hidden layer size at 15 is the starting point of MSE lower until to 25. It is observed that, the MSE for hidden layer size is range between 0.0081 and 0.2520. Hidden layer size at 20 provides lowest MSE with 0.0081. The hidden layer size of 20 is used to adjust the next parameter in the training cycle.

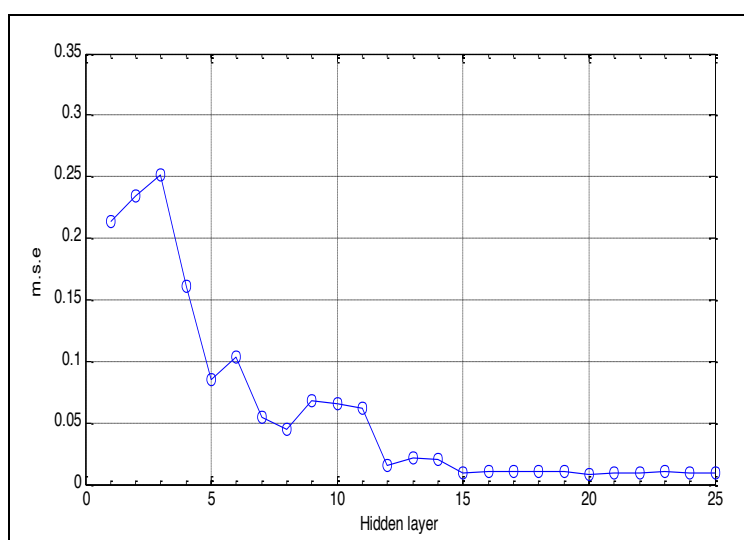
**Figure 2.** ANN final training errors with varying hidden layer

Figure 3 shows the ANN final training errors with varying learning rate. The learning rate is varies from 0.1 to 1. Graphically, it can be seen that the learning rate at 0.3 has minimum MSE. It is observed that, the MSE for learning rate is range between 0.008 and 0.0099, which is very small. Learning rate at 0.3 provides lowest MSE with 0.008. The hidden layer size at 20 and learning rate at 0.3 are used to adjust the momentum rate for ANN training network.

Figure **Error! Reference source not found.**4 shows the ANN final training errors with varying momentum rate. The momentum rate is varies from 0.1 to 1. Graphically, it can be seen that the learning rate at 0.5 has minimum MSE It is observed that, the MSE for momentum rate is range between 0.0076 and 0.0098, which is very small. Learning rate at 0.5 provides lowest MSE with 0.0076.

The optimum ANN network for predicting of three group of stroke level defined with 20 nodes in the hidden layer, a learning rate of 0.3, a momentum rate of 0.5 and best training

performance is 0.0093775 at epoch 36. The training convergence of this network is shown in Figure 5.

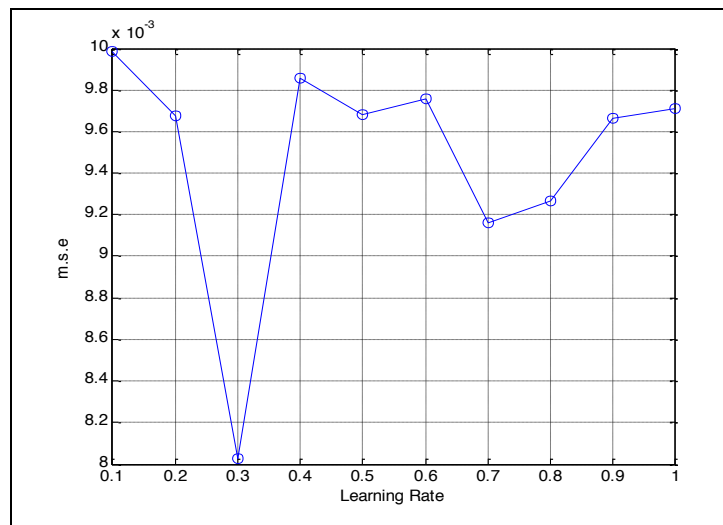


Figure 3. ANN final training errors with varying Learning rate

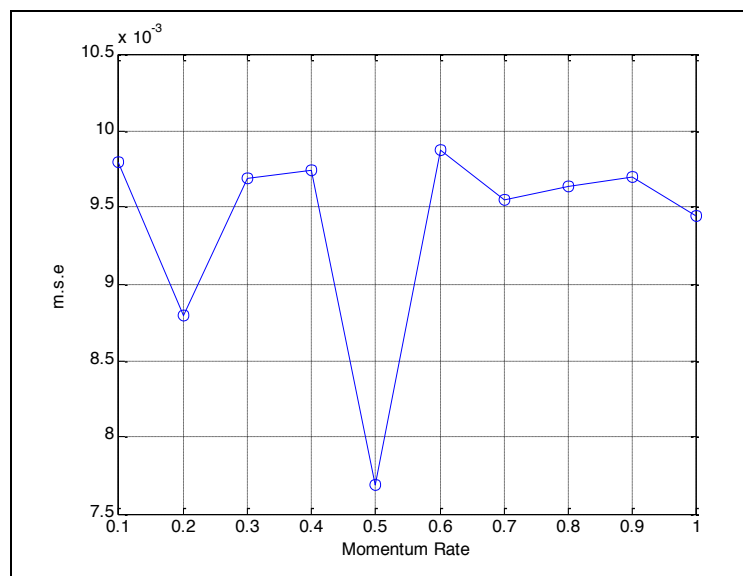


Figure 4. ANN final training errors with varying momentum rate

Table 2 summarizes the ANN final design parameters for the ANN architecture and training parameters. The nodes in input layer is set as 4 (Beta, Alpha, Theta and Delta) and the output layer is 1 which is the stroke severity AG (1), IG (2) or EG (3). The error goal used is 0.01 with the epochs is 100. The other adjusted parameters such as nodes in hidden layer, learning rate, momentum rate and are optimum at 20, 0.3 and 0.5 respectively.

Figure 5 shows the ANN prediction for the training network using the optimized parameters. The training network predicted shows three groups being predicted which is 1, 2 and 3 which refer to AG, IG and EG group of stroke severity, respectively. The first group is less than 1.5; second group between 1.5 to 2.5 and third group is more than 2.55 to 3.5. All the targets are inside the range, therefore no errors are observed.

Table 2. ANN final design parameters

Parameters	Value
Nodes in input layer	4
Nodes in hidden layer size	20
Output layer size	1
Learning rate	0.3
Momentum rate	0.5
Error goal	0.01
Epochs	100
MSE train	0.0097
MSE test	0.4409

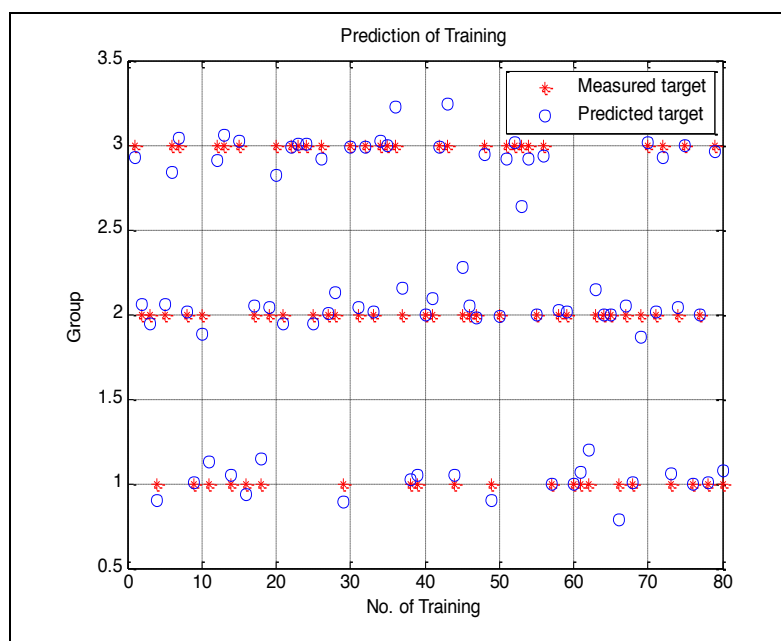
**Figure 5.** ANN prediction for the training network

Figure 6 shows the prediction of the ANN testing using the optimised training network. It is clear that the predicted targets fall under three groups such as 1, 2 and 3. Nevertheless, there are three predicted target are outside target range. The cases are not classified at all.

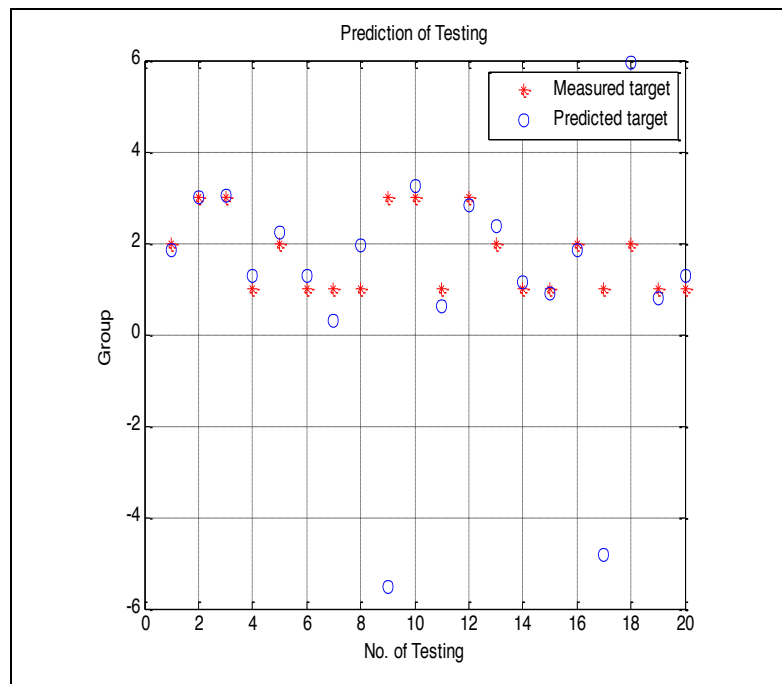


Figure 6. ANN testing prediction

From the quantum efficiency in Figure 2 (b), it also show that the more thickly the active layer, the higher the quantum efficiency. The quantum efficiency (QE) is only affected by the amount of the absorption light. When the active layer is thicker, more light will be absorbed to generate more photocurrent. The QE drop till 0 at around wavelength of 580nm because there are no more light absorbed at higher wavelength.

CONCLUSION

The study showed that the application of ANN in analysing the stroke severity has been successful. The result obtained demonstrates the capability of ANN in predicting the stroke severity into 3 groups. The significant brainwave are identified i.e. Beta, Alpha, Theta and Delta are useful and beneficial for further analysis such as grouping and classification system of stroke severity. Therefore a new technique by using the EEG is an alternative method for describing patients characteristic, behaviour and classifying stroke severity.

Acknowledgments

The authors would like to express gratitude to the Ministry of Higher Education for providing support through the scholarship, representative from NASAM Staffs and stroke patients who cooperated so willingly during data collection and Advanced Signal Processing Research Group (ASPRG) FKE, UiTM for their support and also financial sponsored by UiTM for RIF Grant (600-RMI/DANA 5/3/RIF (8/2012)) and CMET Grant PSA.

REFERENCES

- [1] Borah, S., Hines, E.L., Leeson, M.S., Iliescu, D.D., Bhuyan, M. and Gardner, J.W., (2008). Neural network based electronic nose for classification of tea aroma. *Sensing and instrumentation for food quality and safety*, **2**(1): 7-14.
- [2] Markom, M.A., Shakaff, A.M., Adom, A.H., Ahmad, M.N., Hidayat, W., Abdullah, A.H. and Fikri, N.A., (2009). Intelligent electronic nose system for basal stem rot disease detection. *Computers and Electronics in Agriculture*, **66**(2): 140-146.
- [3] Nakamoto, T., Fukuda, A. and Moriizumi, T., (1991) Perfume and flavor identification by odor sensing system using quartz-resonator sensor array and neural-network pattern recognition. In *Solid-State Sensors and Actuators, 1991. Digest of Technical Papers, TRANSDUCERS'91., 1991 International Conference on*, pp. 355-358.
- [4] Wang, P., Chen, X., Xu, F., Lu, D., Cai, W., Ying, K., Wang, Y. and Hu, Y., (2008). Development of electronic nose for diagnosis of lung cancer at early atage. In *Information Technology and Applications in Biomedicine, 2008. ITAB 2008. International Conference on*, pp. 588-591.
- [5] Scanzio, S., Cumani, S., Gemello, R., Mana, F. and Laface, P., (2010). Parallel implementation of artificial neural network training for speech recognition. *Pattern Recognition Letters*, **31**(11): 1302-1309.
- [6] Majewski, M. and Zurada, J.M., (2008). Sentence recognition using artificial neural networks. *Knowledge-Based Systems*, **21**(7): 629-635.
- [7] Isa, N.A.M. and Mamat, W.M.F.W., (2011). Clustered-hybrid multilayer perceptron network for pattern recognition application. *Applied Soft Computing*, **11**(1): 1457-1466.
- [8] Kamrunnahar, M. and Urquidi-Macdonald, M., (2011). Prediction of corrosion behaviour of Alloy 22 using neural network as a data mining tool. *Corrosion science*, **53**(3): 961-967.
- [9] Sovierzoski, M.A., Argoud, F.I.M. and de Azevedo, F.M., (2008). Evaluation of ANN classifiers during supervised training with roc analysis and cross validation. In *BioMedical Engineering and Informatics, 2008. BMEI 2008. International Conference on*, **1**: 274-278).
- [10] Hobson, R.S., Clausi, A., Oh, T. and Guiseppi-Elie, A., (2003). Temperature correction to chemoresistive sensors in an e-NOSE-ANN system. *IEEE sensors journal*, **3**(4): 484-489.
- [11] Penny, W. and Frost, D., (1996). Neural networks in clinical medicine. *Medical Decision Making*, **16**(4): 386-398.
- [12] Ibrahim, F., Taib, M.N., Abas, W.A.B.W., Guan, C.C. and Sulaiman, S., (2005). *A novel dengue fever (DF) and dengue haemorrhagic fever (DHF) analysis using artificial neural network (ANN)*. *Computer methods and programs in biomedicine*, **79**(3): 273-281.
- [13] Khan, J., Wei, J.S., Ringner, M., Saal, L.H., Ladanyi, M., Westermann, F., Berthold, F., Schwab, M., Antonescu, C.R., Peterson, C. and Meltzer, P.S., (2001). Classification and diagnostic prediction of cancers using gene expression profiling and artificial neural networks. *Nature medicine*, **7**(6): 673-679.
- [14] Zadeh, A.E., Khazae, A. and Ranaee, V., (2010). Classification of the electrocardiogram signals using supervised classifiers and efficient features. *computer methods and programs in biomedicine*, **99**(2): 179-194.

- [15] Omar, W.R.W., Jailani, R., Taib, M.N., Isa, R.M. and Sharif, Z., (2013). Assessment of acute ischemic stroke brainwave using Relative Power Ratio. In *Signal Processing and its Applications (CSPA), 2013 IEEE 9th International Colloquium on*, pp. 310-313.
- [16] Fatourehchi, M., Bashashati, A., Ward, R.K. and Birch, G.E., (2007). EMG and EOG artifacts in brain computer interface systems: A survey. *Clinical neurophysiology*, **118**(3): 480-494.
- [17] Nolan, H., Whelan, R. and Reilly, R.B., (2010). FASTER: fully automated statistical thresholding for EEG artifact rejection. *Journal of neuroscience methods*, **192**(1): 152-162.

Humanoid Robot Navigation in Human Environment

Zulkifli Mohamed¹, Genci Capi^{2*}

Faculty of Mechanical Engineering, Universiti Teknologi MARA, 40450, Shah Alam, Selangor DE, Malaysia.

(*corresponding author: zulkifli127@salam.uitm.edu.my)

Received: 11.10.2015 ; accepted 19.12.2015

Abstract Manoeuvring in human environment is a great challenge for a mobile humanoid robot. The humanoid robot is required to move from an initial point to a desired location while avoiding obstacles. In order to operate in such environments, the robot must be able to navigate and interact with human. This paper present a mobile humanoid robot that is able to localize itself, navigate to the target location. The robot utilizes laser sensor, camera and compass sensor for localization and navigation. In addition, the robot has the abilities to avoid moving object and human along the way. The evolved neural controllers generate humanoid robot navigation optimizing the distance and simultaneously avoid any obstacles along the pathway. An advantage of proposed method is that in a single ran of Multi-Objective Genetic Algorithm, multiple neural controllers are generated.

Keywords Mobile Humanoid Robot Navigation; Multi-Objective Genetic Algorithm; Intelligent System

INTRODUCTION

In order to perform a navigation task such as getting a bottle of milk from the kitchen or guiding humans from one location to another, many considerations need to be made such as understanding the command, determining the environment, obstacles avoidance, object recognition and manipulation and human safety. Direct contact between human and robot has been proposed by [1], [2] to guide the human from one location to another, for example leading a child to their parents or assisting patients in hospitals. A combination of MEKA Robotic arms, an Omni directional Segway and a linear actuator by Festo are utilized as complete robotic system. A nurse robot, PEARL has been presented in [3] for assisting the elderly. Two main purpose of PEARL is to remind people about routine activities such eating, drinking, bathing and taking medicine and the other function is to guide them through their environment. In [4], a robot called “Dynamaid” adapted four schemes for navigation namely Fast Simultaneously Localization and Mapping (FastSLAM), localization, path planning and safe local navigation. Holz et al. [5], has proposed global-to-local control strategy to navigate the developed robot, Cosero from the transport box to the processing place for bin picking. Adaptive Monte Carlo Localization is used to estimate the robot’s pose in a given grid map using LRF. A* search is applied to find the shortest obstacles free path from the estimate position to the target location. In his paper, the application of multi objective evolutionary algorithm for humanoid robot navigation is presented. The robot utilizes the sensors data such as LRF, camera and compass to navigate in the environment. Multi-objective evolutionary algorithm is utilized to generate optimal neural controllers for the robot

navigation from the elevator into the lab. The performance of evolved neural controllers is tested on the mobile humanoid robot developed in our lab.

METHODOLOGY

Mobile Humanoid Robot

The detail descriptions of the developed mobile humanoid robot are discussed in terms of its kinematics analysis, mechatronics design and software configuration in [6]. The design of the mobile humanoid robot considers the safety features, ability to navigate throughout the environment, obstacles avoidance, object recognition and the ability to perform object manipulation tasks [7 - 8]. The robot system is divided into two main parts, the upper body and the mobile platform. The upper body is designed mainly for object manipulation, while the mobile platform is utilized for the robot navigation. The mobile platform is powered by two AC motors with 24V battery, a controller and base for the upper body. The battery, PC, AC motors, Laser Range Finder (LRF) and the upper body is placed on this platform, as shown in Figure 1. The mobile platform has a maximum speed of 1 ms^{-1} and it can be easily controlled using MATLAB based PC. LRF is utilized for robot navigation which can scan from 2 cm to 560 cm in distance with 240° range. The accuracy of the measured distance is within 3% at 100 ms/scan and the scanning resolution is 0.360. The LRF has weights 160 g and it is powered by 5V voltage supply.

Mobile Humanoid Robot

In this work, the environment where the robot will operate is known. However, the environment is considered dynamic with moving and stationary obstacles. We evolved neural controllers for 3 different environments as shown in Figure 2. The robot has to navigate from the elevator into the lab room with minimum distance travelled. A Feed Forward Neural Network (FFNN) is utilized for the robot navigation with 16 inputs from LRF, 6 hidden units and a single output for robot steering (Figure 3). Multi objective genetic algorithm (MOGA) is utilized to optimize the connection weight of the FFNN [9].

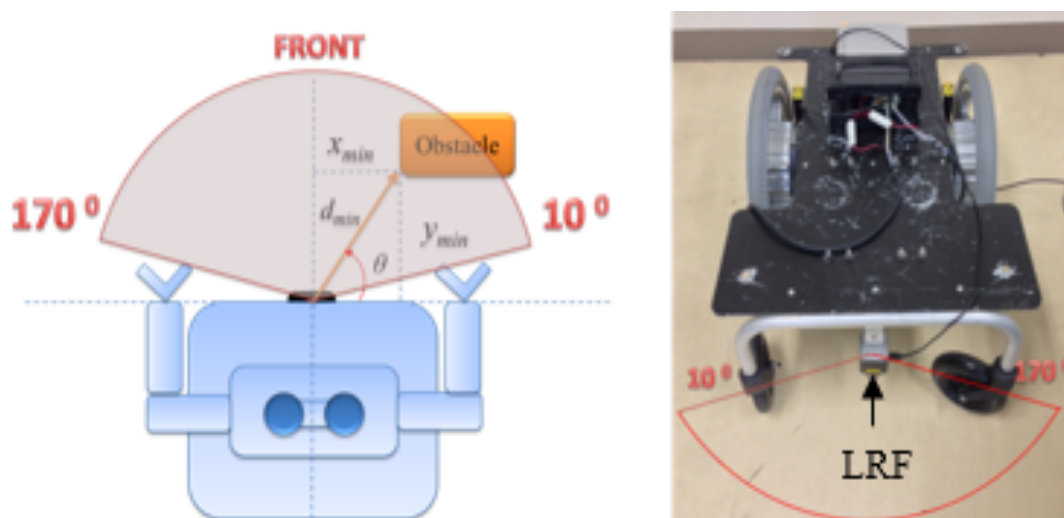


Figure 1. Mobile Platform



(a)

(b)

Figure 2. Robot navigation (a) Simulation (b) Real environments

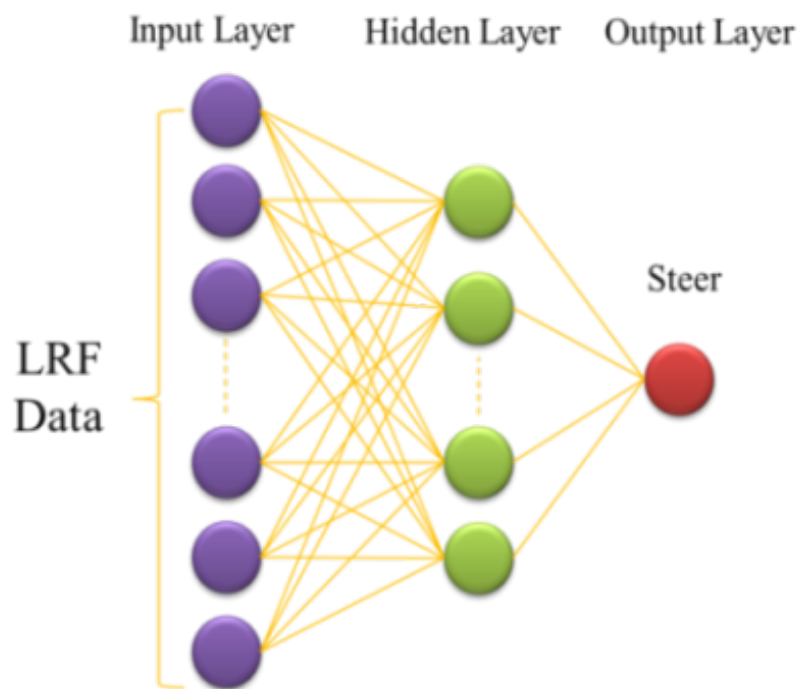


Figure 3. FFNN for mobile platform

Objective Function

1. *Environment I*: The robot is required to move from the elevator (point 1) to the middle of the hallway (point 2) in a shortest distance while avoiding obstacles. The fitness function utilized is as follow:

$$f_1 = \sqrt{(x_2 - x_1)^2 + (y_2 - y_1)^2} + \frac{sensor_{side}}{n_{step}} \quad (1)$$

Where x_1 and y_1 is the position of the robot at point 1, x_2 and y_2 is the position of the robot at point 2, $sensor_{side}$ is the differences between the left and the right reading of LRF and n_{step} is the number of step.

2. *Environment II*: In the next environment, the robot has to maneuver from the starting point of the hallway (point 2) to the entrance of the goal position (point 3). The shortest distance between two points in the horizontal x direction is optimized and the sensor data is used for obstacles avoidance and guiding the robot to be in the center line of the hallway. The fitness function for environment 2 is as follows.

$$f_2 = x_3 - x_2 + \frac{sensor_{side}}{n_{step}} \quad (2)$$

Where x_2 and y_2 is the position of the robot at point 2, x_3 and y_3 is the position of the robot at point 3 (the goal position entrance).

3. *Environment III*: In environment 3, the robot will determine the desired entrance door to the goal position based on the landmark placed on top of the door. This is similar as in a hospital or a care center where each room will have the room number or its own specific landmarks. In our implementation, a colour landmark is utilized and it will be detected using the robot camera. The size of the colour landmark is 180 mm x 320 mm and it is place 2 m from the floor. The fitness function for the neural controllers is shown below:

$$f_3 = \sqrt{(x_4 - x_3)^2 + (y_4 - y_3)^2} \quad (3)$$

Where x_3 and y_3 is the position of the robot at point 3, x_4 and y_4 is the position of the robot at point 4 (the goal position). This function is optimizing the distance between point

3 and 4 while avoiding the door and table inside the room. The door size is 900 mm and it is slightly narrow for the robot to enter with 520 mm width.

RESULTS AND DISCUSSION

The performance of neural controllers generated in the simulation is tested on the real robot. The robot moves from the initial to the goal location by switching to the appropriate neural controller. In environment 1, there are some differences between simulation and real robot navigation. This is due to some glass doors which are not detected by the LRF. Simulated result shows shorter and smoother trajectory from the starting point 1 to point 2 comparing to the real robot motion (Figure 4(a)). The total distance of the real robot is slightly higher but manages to reach the target location successfully. Out of 20 trials that have been carried out, 95% the robot manage to reach at the center of the hallway. Figure 4(b) shows the video capture of the real robot motion in environment 1. As the robot reaches the environment 2, the robot switches to the next neural controller. The result show good performance in both simulation and on the real robot (Figure 5(a)).

The robot has to move in a straight hallway avoiding a book rack before it reach the third environment. The real robot has the ability to move in a similar distance and trajectory as in simulated environment. Figure 5(b) shows the robot motion along the hallway while avoiding the book rack. Out of 20 trials that have been carried out, 95% the robot manage to reach point 3 successfully. In the third environment the robot has some difficulties to execute the task. The robot needs to enter the room through a 95cm door and stop near the table for manipulation task. Figure 6(a) shows the best result and the real robot move in a slightly in the inner section compares to the simulation result. In this environment, the successful rate of the robot reaching the goal position is reduced. Figure 6(b) shows the video capture of the real robot entering the room. The successful rate of the robot entering the room is 80% out of 20 trials. All paragraphs must be indented. All paragraphs must be justified, i.e. both left-justified and right-justified.

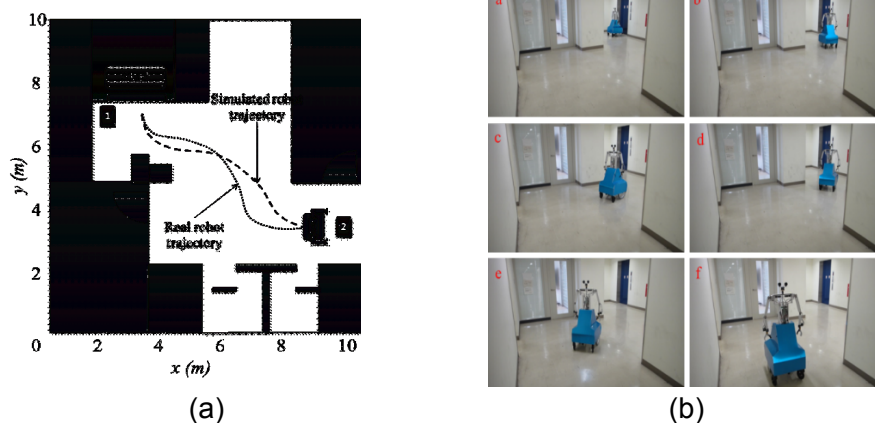


Figure 4. Robot navigation in environment 1 for (a) Simulation (b) Experiment

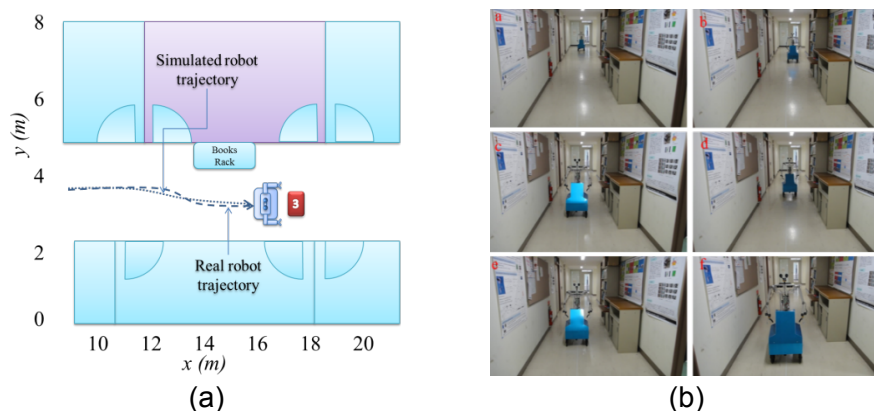


Figure 5. Robot navigation in environment 2 for (a) Simulation (b) Experiment

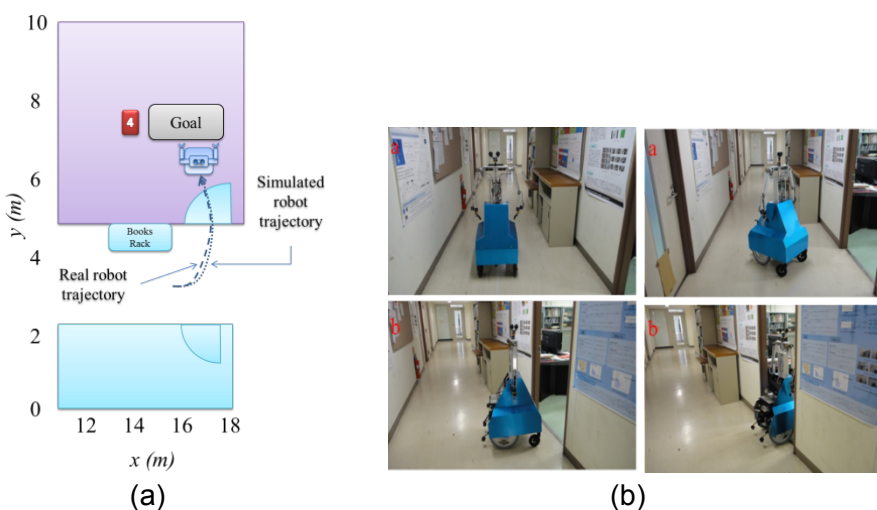


Figure 6. Robot navigation in environment 3 for (a) Simulation (b) Experiment

CONCLUSION

This paper presented an intelligent mobile humanoid robot for assistive tasks focusing on robot navigation. The evolved neural controller show good performance both in simulation and on the real robot. The mobile robot was able to reach the goal by switching to the appropriate neural network. Results show that although there are some small differences between simulations and experiments the robot completed the task successfully.

REFERENCES

- [1] Chen, T.L. and Kemp, C.C., (2010), March. Lead me by the hand: Evaluation of a direct physical interface for nursing assistant robots. In *Human-Robot Interaction (HRI), 2010 5th ACM/IEEE International Conference on*, pp. 367-374.
- [2] King, C.H., Chen, T.L., Jain, A. and Kemp, C.C., (2010), October. Towards an assistive robot that autonomously performs bed baths for patient hygiene. In *Intelligent Robots and Systems (IROS), 2010 IEEE/RSJ International Conference on*, pp. 319-324.

- [3] Pollack, M.E., Brown, L., Colbry, D., Orosz, C., Peintner, B., Ramakrishnan, S., Engberg, S., Matthews, J.T., Dunbar-Jacob, J., McCarthy, C.E. and Thrun, S., (2002), August. Pearl: A mobile robotic assistant for the elderly. In *Workshop on Automation as Caregiver: the Role of Intelligent Technology in Elder Care (AAAI)*, pp. 85-91.
- [4] Stückler, J., Gräve, K., Kläß, J., Muszynski, S., Schreiber, M., Tischler, O., Waldukat, R. and Behnke, S., (2009), June. Dynamaid: Towards a personal robot that helps with household chores. In *Robotics: science and systems conference (RSS'09)*.
- [5] Holz, D., Nieuwenhuisen, M., Droeschel, D., Stückler, J., Berner, A., Li, J., Klein, R. and Behnke, S., (2014). Active recognition and manipulation for mobile robot bin picking. In *Springer Tracts in Advanced Robotics (STAR)*, pp. 133-153.
- [6] Mohamed, Z. and Capi, G., (2012). Development of a new mobile humanoid robot for assisting elderly people. *Procedia Engineering*, **41**: 345-351.
- [7] Mohamed, Z., Kitani, M., Kaneko, S.I. and Capi, G., (2014). Humanoid robot arm performance optimization using multi objective evolutionary algorithm. *International Journal of Control, Automation and Systems*, **12**(4): 870-877.
- [8] Mohamed, Z., Kitani, M. and Capi, G., (2014). Adaptive arm motion generation of humanoid robot operating in dynamic environments. *Industrial Robot: An International Journal*, **41**(2): 124-134.
- [9] Capi, G., (2007). Multiobjective evolution of neural controllers and task complexity. *IEEE Transactions on Robotics*, **23**(6): 1225-1234.